Nanoscale

Accepted Manuscript

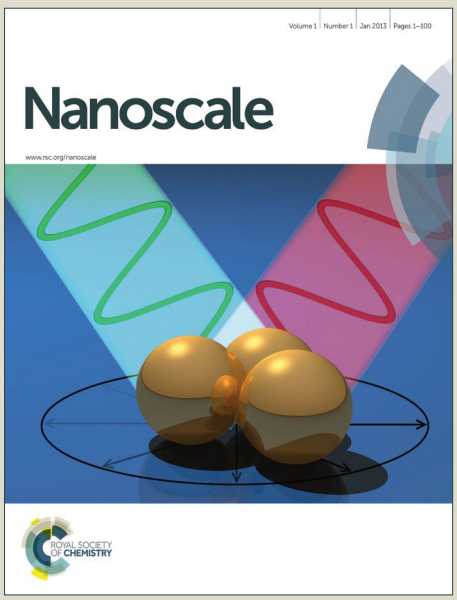

ROYAL SOCIETY OF CHEMISTRY

www.rsc.org/nanoscale

Nanoscale

RSCPublishing

ARTICLE

Nanocomposite heterojunctions as sunlight-driven photocatalysts for hydrogen production from water splitting

Cite this: DOI: 10.1039/x0xx00000x

Received 00th January 2012,
Accepted 00th January 2012

DOI: 10.1039/x0xx00000x

www.rsc.org/

Mohammad Reza Gholipour,[a] Cao-Thang Dinh,[a] François Béland[b] and Trong-On Do[a,*]

Hydrogen production via photocatalytic water splitting using sunlight has an enormous potential to solve the worldwide energy and environmental crisis. The key challenge in this process is to develop efficient photocatalysts which must satisfy several criteria such as highly chemical and photochemical stability, effective charge separation and strong sunlight absorption. Combination of different semiconductors to create composite materials offers a promising way to achieve efficient photocatalysts because it can improve the charge separation, light absorption and stability of the photocatalysts. In this review article, we summarized the most recent studies on semiconductor composites for hydrogen production under visible light irradiation. After a general introduction about photocatalysis phenomenon, typical heterojunctions of widely studied heterogeneous semiconductors, including titanium dioxide, cadmium sulfide and graphitic carbon nitride are discussed in details.

1. Introduction

Nowadays, fossil fuels play an important role in human life and provide worldwide energy demands because of their low cost and availability. They evolved from prehistoric fossils over hundreds of years and would no longer available if once used. Moreover, the combustion of these fossil fuels produces tons of air pollution gases such as nitrogen oxides, sulfur oxides and carbon oxides annually which cause severe health problems for humans and global climate change. Finding renewable, clean and carbon-neutral alternative energy sources is thus urgently needed.

Among various available renewable energy sources, solar energy is by far the most abundant one. It is estimated that around 0.01% energy of one-second sunlight irradiation is sufficient to annual energy consumption of human society.[1, 2] However, a significant challenge is to put this kind of energy into practice and store it for later application. One of the promising ways is using hydrogen as energy carriers in order to store solar energy in the form of chemical bond between two atoms of hydrogen. Then, this hydrogen molecule can react with oxygen in the air to release its energy and produce water as a by-product, which is totally clean for the environment.

Water is the most plentiful supply of hydrogen that can be used to produce hydrogen via photocatalytic water splitting. Thus, hydrogen production by means of photocatalyst, solar energy and water has been attracted noticeably for recent decades. This technology is clean because it uses photon energy and water. Besides, it doesn't produce any dangerous by-products or pollutants. Therefore, photocatalysis process is expected to make a great contribution to energy and environmental challenges in the near future.

The most challenging task in photocatalytic water splitting is to develop efficient photocatalysts which are capable of adsorbing the sunlight to split the water. In general, photocatalysis involves three processes: the excitation, bulk diffusion and surface transfer of photoinduced charge carriers. Thus, an efficient photocatalyst must satisfy several critical requirements related to its semiconducting and chemical properties, its crystalline structure and surface characteristics. However, there are always inherent deficiencies of the semiconductors, and it is very difficult to find a single component that can address all of these requirements. Thus, although many different semiconductors for water splitting have been developed in the last decades, most of them are activated under UV light and need sacrificial reagents to produce hydrogen from water. It seems that single component photocatalyst, even with cocatalysts, cannot obtain desirable quantum efficiency.

Semiconductor/semiconductor heterojunction, formed by the direct contact of two semiconductors, represents an effective architecture for overcoming the limit of single component photocatalysts. When the two semiconductors with suitable band edge positions are combined, the charge transfer between them can increase the lifetime of the charge carriers, thus promoting the photocatalytic process. In addition, when the band gap of the coupled semiconductor is small, the energy range of photo-excitation for the system is also extended. In this review paper, we summarized various nanocomposite photocatalysts which were activated for hydrogen production under visible light illumination.

2. Fundamentals of Photocatalytic water splitting

Fujishima and Honda were pioneers in decomposing water with light illumination.[3] They discovered that TiO_2 and Pt can act as anode and cathode electrodes, respectively, in a photoelectrochemical cell. This system could split water into hydrogen and oxygen under intense UV irradiation. Some years later, Bard applied the concept of this system to introduce photocatalysis process.[4] Since then, there have been enormous efforts on developing semiconductors that can decompose water into H_2 and O_2 under the light illumination.

Generally, photocatalytic water splitting with sunlight consists of three main steps: (I) a semiconductor absorbs light photons and generates excited electrons and holes; (II) these excited electrons and holes can migrate to the surface of semiconductor or recombine again inside the bulk material; (III) on the surface, holes can oxidize water to O_2 (Equation.1) and electrons can reduce protons to H_2 (Equation.2). Figure 1 illustrates schematically the main steps in water splitting.

$$H_2O + 2h^+ \rightarrow \frac{1}{2}O_2 + 2H^+ \quad (1)$$

$$2H^+ + 2e^- \rightarrow H_2 \quad (2)$$

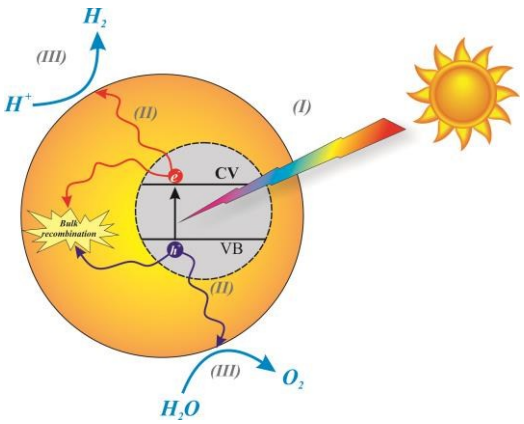

Figure 1: Schematic fundamental mechanisms of photocatalytic water splitting.

Semiconductor band gap determines which wavelength of sunlight can be absorbed. The semiconductor with a wide band gap (E_{bg} > 3 eV) can only absorb UV light, which approximately accounts for 5% of solar energy. In contrast, a narrow band gap semiconductor (E_{bg} < 3 eV) can be activated by visible light irradiation, which constitutes 43% of the sunlight spectrum. Beside band gap, the positions of the valence and conduction bands are also very important in photocatalytic water splitting. For H_2 evolution, the conduction-band edge should be more negative than the reduction potential of H^+ to H_2 ($E_{H^+/H_2} = 0\ V\ vs\ NHE\ at\ pH = 0$). On the other hand, the valence-band edge should be more positive than the oxidation potential of water ($E_{O_2/H_2O} = 1.23\ V\ vs\ NHE\ at\ pH = 0$) in order to evolve oxygen. Therefore, the band gap of semiconductor should be at least 1.23 eV in order to split the water. The equivalent light wavelength for this band gap energy is 1100 nm, which is in near-infrared region of the sunlight spectrum. By considering other factors such as energy losses during different stages in the photocatalytic process, effective semiconductors should have band gaps greater than 2 eV, which is related to the light with wavelength less than 620 nm.[5, 6] Although some semiconductors can absorb the infrared light by photon up-conversion mechanism, their applications are usually limited to degradation of organic compounds.[7-10]

2.1. Overall water splitting

Decompose water directly into hydrogen and oxygen under sunlight irradiation is the ultimate goal of photocatalytic hydrogen generation system. In this process, a semiconductor with proper band-edges can absorb photon energy and evolve hydrogen and oxygen simultaneously. However, this reaction is thermodynamically non-spontaneous with the Gibbs free energy of 237 kJ/mol.[11]

$$2H_2O \xrightarrow{photon\ energy} 2H_2 + O_2 \quad (3)$$

Some semiconductors can absorb UV light and split water directly into hydrogen and oxygen, but most of them have an energy conversion efficiency less than 1%.[12-14] Moreover, they cannot produce hydrogen and oxygen in a stoichiometric ratio because one type of charge carriers is accumulated on the surface of photocatalyst.[11] One exceptional example is a GaN-ZnO solid solution photocatalyst that can split water into hydrogen and oxygen stoichiometrically under visible light illumination with a quantum efficiency of about 6%.[15] It is obvious that overall water splitting is very difficult to be proceeded under visible light illumination and becomes one of the greatest challenging for researchers in this field.

2.2. Sacrificial reagent systems

As discussed earlier, the overall water splitting is a very hard reaction to be proceeded, and it needs a specific kind of semiconductor with appropriate band edge positions. Nevertheless, some semiconductors can do one of the half reactions of water splitting, i.e. water reduction or oxidation, in the presence of suitable sacrificial reagents (electron donors or acceptors). In principle, sacrificial agents usually react with one type of charge carriers while the other carrier reacts with water to produce hydrogen or oxygen. Electron donors, which consume excited holes on the surface of the semiconductor, are used for water reduction half reaction and electron acceptors (electron scavengers) are usually needed for water oxidation, as illustrated in Figure 2. Generally, the electron donors must be more readily oxidized than water by excited holes, while the electron acceptors must be more readily reduced than water by excited electrons. The most common electron donors are methanol, ethanol, triethanolamine (TEA) and an aqueous solution of Na_2S/Na_2SO_3, whereas metal cations such as Ag^+ and Fe^{3+} are usually utilized as electron acceptors.[11]

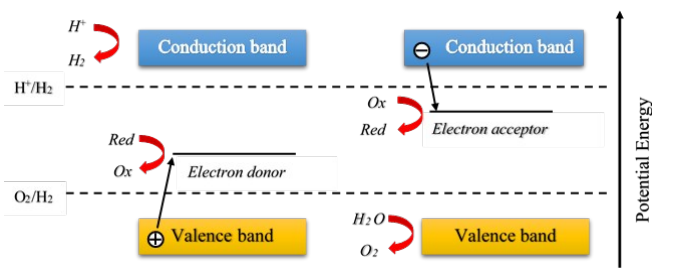

Figure 2: Schematic principles of water reduction or oxidation in the presence of sacrificial reagents.

Various mechanisms have been proposed to explain the consumption of sacrificial reagents in hydrogen production reactions.[14,16] These electron donors react more easily with holes than water due to its less positive oxidation potential. This would lead to accelerated holes consumption on the surface of the photocatalyst and so the positive charge accumulation is partially prevented and, as a result, protons and

photoexcited electrons can react together more easily. It should be noted that, in the case of using methanol as electron donor, hydrogen is also produced from water as a result of methanol conversion (Equation.4).[17,18] However, by increasing the carbon chain, the contribution of H_2 production from alcohol conversions decrease substantially.[18] Moreover, Guzman showed that the direct reaction of methanol with holes does not proceed to an appreciable extent in the presence of high concentration of water.[19]

$$CH_3OH + H_2O \rightarrow CO_2 + 3H_2 \qquad (4)$$

Semiconductors capable of decomposing water in the presence of sacrificial agents may seem to be useless. Nevertheless, these photocatalysts not only can be used in Z-schematic system but also some of them can be used to produce H_2 using biomass derived sacrificial reagents.[20,21]

2.3. Electron mediator systems

The electron mediator system is also called Z-scheme system or a dual photocatalyst system. The concept of this system is to transfer charge carriers by two different electron mediators in a solution and after participating in redox reactions, they all return to their original chemical states.[22] This procedure for overall water splitting is entirely different than two previous methods. It needs two various photocatalysts: a semiconductor provides photoexcited electrons to participate in half-reaction for H_2 evolution; another one supplies photogenerated holes to take part in half-reaction of water oxidation. Moreover, two semiconductors should be excited simultaneously and one half of charge carrier will recombine in order to bring electron mediator in their original states (Figure 3). Some of the most common electron mediators are Fe^{3+}/Fe^{2+}, IO^{3-}/I^- and Ce^{4+}/Ce^{3+}.[23]

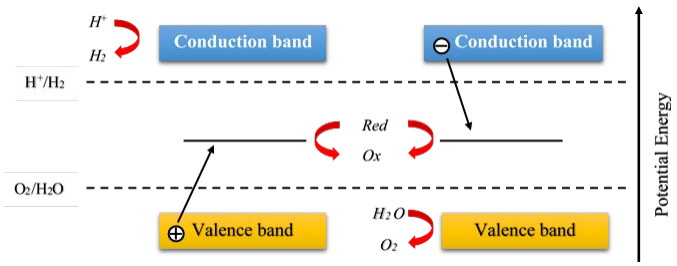

Figure 3: Schematic principles of overall water splitting in the Z-scheme system.

There are some review papers discussing different approaches and application of this dual step system, which is similar to plant photosynthesis.[24, 25] Nonetheless, this system has some drawbacks in comparison with one-step system. For instance, Z-scheme system are usually more complicated and it needs more photons to produce the same amount of hydrogen because half of the excited charges are used in order to bring the excited mediator to its ground state for further reactions.[22, 26]

2.4. Activity and quantum efficiency

Photocatalytic activity depends on many factors such as light source (Xe or Hg lamps), light intensity, reaction cell, different directions of irradiation (top, inner, or side), reaction media (water or various sacrificial agents), and the quantity of photocatalyst. The simplest way to find semiconductor activity is to measure the amount of evolved gases in a specific period of time and report it in $\mu mol \cdot h^{-1}$ or $\mu mol \cdot h^{-1} \cdot g^{-1}$ units.[23]
Quantum yield (Quantum efficiency) is another way to report photocatalytic activity of a semiconductor. This is independent of affective factors that are mentioned above and it is defined as:[27]

$$Quantum\ yield\ (\%) = \frac{Number\ of\ reacted\ electrons}{Number\ of\ absorbed\ photons} \times 100 \qquad (11)$$

Despite this equation can give us accurate quantum yield, it is very hard to measure the real amount of absorbed photons. In order to solve this problem, researchers suggested to use apparent quantum yield, which is declared as follows:[23]

$$\begin{aligned} &Apparent\ quantum\ yield\ (\%) \\ &= \frac{Number\ of\ reacted\ electrons}{Number\ of\ incident\ photons} \times 100\% \\ &= \frac{2 \times Number\ of\ evolved\ H2\ molecules}{Number\ of\ incident\ photons} \times 100\% \\ &= \frac{4 \times Number\ of\ evolved\ O2\ molecules}{Number\ of\ incident\ photons} \times 100 \end{aligned} \qquad (12)$$

It is obvious that the apparent quantum yield is smaller than the real quantum efficiency because of the difference between the number of absorbed photons and incident light.
Solar energy conversion efficiency is a method to calculate solar cell efficiency, it can also be used to report the photocatalytic activity of a semiconductor.

$$Solar\ energy\ conversion\ efficiency\ (\%) = \frac{Output\ energy\ of\ H2\ evolved}{Energy\ of\ incident\ solar\ light} \times 100\% \qquad (13)$$

Up to now, semiconductors have extremely low solar energy conversion values and so this indicator is seldom used.[12] It is anticipated that for industrial application of water splitting via sunlight, this efficiency should improve noticeably.

2.5. Cocatalysts

A cocatalyst is a compound added to the semiconductors photocatalyst to improve their activity. In photocatalytic water splitting, the cocatalysts can be used to enhance either the water oxidation or reduction reactions. The cocatalyst for water reduction are usually small metal nanoparticles which can form Schottky junction with semiconductors and enhance charge separation in photocatalyst or photoelectrochemical cell.[28, 29] In principle, the contact between metal and semiconductor creates an electric field that separate excited electrons and holes more easily, as demonstrated in Figure 4.[30-32] If the work function of metal matches the conduction band-edge of semiconductor, excited electrons move from the semiconductor to the metal and from there, they can react with water. In addition, the metal provides active sites for hydrogen generation due to its relatively low over-potential for water reduction.
The physical and chemical properties of cocatalyst such as particle size and valence states, which significantly affect their performance, are strongly dependent on the loading method of cocatalysts. Although depositing more cocatalysts provide more active sites for reactions, they reduce the absorption ability of the photocatalyst. Therefore, the concentration of cocatalysts should be optimized to obtain the maximum activity during water splitting under light illumination.
There are two main techniques to deposit cocatalysts on the surface of semiconductors: in situ photodeposition and impregnation. In the first one, cocatalyst is reduced by

photoexcited electrons on the surface of a semiconductor under light irradiation in the presence of sacrificial reagents. Therefore, the semiconductor should be mixed with a precursor solution of cocatalyst. If photo-reduction step is performed subsequently with various precursor, core-shell structure can be achieved easily.[33]

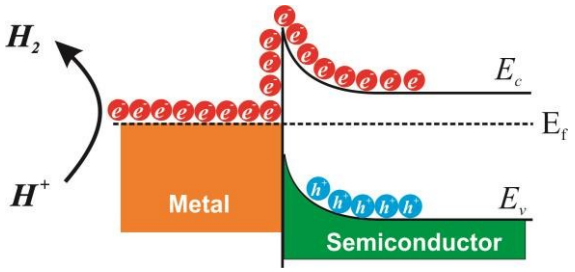

Figure 4: A schematic energy band model of Schottky junction.

The second one is usually followed by post-calcination step. First, a semiconductor is impregnated with a solution containing cocatalyst precursor and then evaporated and dried. After this stage, the dry mixture is calcined in air or other gases such as hydrogen or argon in order to obtain desired states of metal or metal oxide. The final state of cocatalyst depends on gas treatment, temperature and type of precursor.[23]

There have been great efforts to use different types of cocatalysts including transition metals, metal oxides and noble metals for each half reaction of water splitting. The most common cocatalysts for hydrogen evolution are Pt, Rh, Au, NiO[34] and RuO_2. [35-37 38 34 39] Others types such as the core shell configuration of cocatalysts has been recently proposed to improve H_2 evolution in overall water splitting.[33, 40] Although cocatalysts are important part of photocatalytic system, in this review, we only focus on different nanocomposites of semiconductors that are active under visible light illumination.

3. Nanocomposites for visible-light-driven photocatalytic hydrogen production

It is proved that some semiconductor properties such as specific surface area, particle size, crystallinity, crystalline phase and morphology have considerable effects on photocatalytic activity.[41] Charge recombination centers are some kind of defects (in the crystal structure or on the surface of photocatalysts) where photoexcited electrons and holes recombine together.[42] Because of this phenomenon, most of photocatalysts have a very low efficiencies under light irradiation.[43] Even in single crystals (free of defects), the charge recombination process is also possible, due to their non-directional and long-distance migration from inside to the photocatalyst surface. It is noted that excited electrons and holes recombine together less than 10^{-9} s, whereas it takes more time for absorbed species to react with these charges (10^{-8} – 10^{-3} s).[2] If the recombination process can be partly diminished, high efficient photocatalysts are gained for the water splitting reaction.

Scientists have been working on different strategies to enhance charge separation and migration. Nanotechnology has a great advantage for photocatalytic activity due to the fact that the photoexcited charges can migrate considerably shorter distances from the bulk material to the reaction sites on its surface.[7] In addition, the high surface area of nanomaterial results in enhancing chemical adsorption on the surface of nanoparticles and so the possibility of reactants reacting together boosts noticeably. For instance, nano-sized CdS, $LaFeO_3$ and Ta_3N_5 revealed higher photocatalytic activities for H_2 evolution than the bulk ones.[44-47] Nevertheless, by reducing the particle size to nanoscale, surface defects and charge recombination becomes dominant, which compensates the benefits of nanoparticle semiconductors.[48, 49] Therefore, the highest activity was not necessarily achieved with smallest nanocrystals and so the optimal particle size is a key factor for acquiring the highest efficiency of a nano-photocatalyst.[50, 51] It is noteworthy that, in the nanomaterials, crystallinity plays a more dominant role than having a higher surface area.[7]

As seen in Figure 5, the number of publications on nano-photocatalysts have been increased substantially in the last decade, but obviously more work needs to be done in this field in order to find suitable and efficient photocatalysts for hydrogen production.

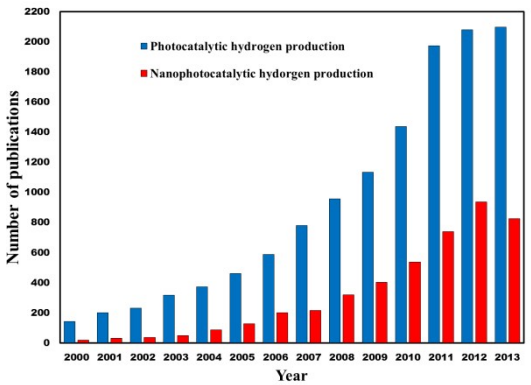

Figure 5: The number of publications on photocatalytic H2 production sorted by year. Data were collected from the "Web of Science".

3.1. Semiconductor heterojunction structures

Instead of using a single semiconductor, combining a semiconductor with other semiconductors, metals, and molecules would lead to form a heterojunction structure between them. These heterojunctions were found to enhance the performance of various devices such as solar cells, photoluminescence and electro-chromic devices.[52-54] In addition, the utilization of nanocomposites as photocatalyst instead of single semiconductor, is another efficient and practicable approaches to enhance the photocatalytic performance. In this kind of nanocomposite, excited charges migrate from one semiconductor to another semiconductor (or metal which act as a cocatalyst). The second semiconductor should have proper band-edge position or higher efficiency in comparison with the first one. Furthermore, this nanocomposite can improve its efficiency due to the fact that reduction and oxidation reactions happen in two different components.[2]

All of heterojunctions can be categorized into three types based on their conduction and valance band positions, as illustrated in Figure 6. In Type 1, both excited electrons and holes move from semiconductor 2 to semiconductor 1 due to their band edge positions. Usually this kind of heterojunction doesn't improve photocatalysts because of accumulation of both charge carriers on one semiconductor.

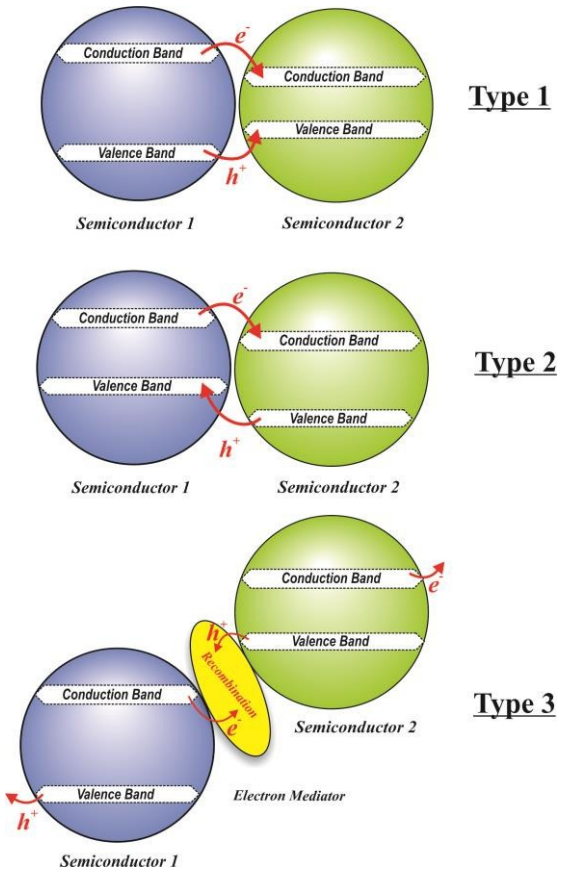

Figure 6: Various kinds of heterojunctions.

In the second group of heterojunctions, the conduction band of semiconductor 1 is lower than that of semiconductor 2. However, the valence band of semiconductor 1 has higher value than that of semiconductor 2. As a result, excited electrons can move from semiconductor 2 to 1, although generated holes migrate vice versa. If both semiconductors have sufficient intimate contacts, an efficient charge separation will occur during light illumination. Consequently, charge recombination is decreased and so charge carriers have longer lifetime, which results in higher photocatalyst activity. Most of the composites discuss in this literature, are type 2.

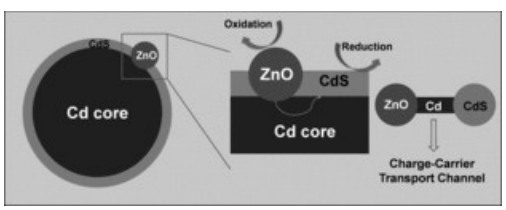

Figure 7: Scheme of the improving mechanism of photoexcited charge-carrier transport in the ZnO–CdS@Cd heterostructure.[55]

Type 3 consists of semiconductors which both valence and conduction bands are lower than the other one, as can be seen from Figure 6. This kind can be applied in the Z-scheme system with an appropriate electron mediator or some kind of bridges that attach two semiconductors. For instance, Wang et al. synthesized a core-shell nanocomposite of ZnO–CdS@Cd in such a way that Cd element acts as the charge-carrier bridge.[55] A schematic of this nanocomposite is demonstrated in Figure 7.

3.2. Various kinds of semiconductors

All of the semiconductors can be classified into 3 main groups based on their properties for hydrogen production: metal oxides, metal sulfides, and metal free semiconductors.

There are different metal oxides that can be utilized as a photocatalyst in a variety of reactions according to their band structures and activities. Most of them are active for hydrogen production under UV light irradiation because of their conduction band positions. Among them, titanium dioxide have attracted the greatest attention of scientists due to its efficiency, high stability, low cost and non-toxicity. However, it can absorb UV light likewise other metal oxides due to its wide band gap. Therefore, this semiconductor has a very low energy conversion from sunlight.

Contrary to metal oxides, metal sulfides usually have narrow band gaps and so they can absorb the energy of photons in visible region. In addition, the conduction band of these semiconductors are more negative than the reduction potential of water and so they can reduce water to hydrogen. Nevertheless, these semiconductors usually consume generated holes to oxidize themselves. Thus, they are unstable during photocatalytic reactions. CdS is one of the best semiconductors with high efficiency for hydrogen production under sunlight irradiation. Due to its instability, the metal sulfide combined with others semiconductors with the aim of improving its stability and photocatalytic efficiency.

Besides these semiconductors, some nitrides also show photo-activity for hydrogen production in visible range of sunlight spectrum. Recently, graphitic carbon nitride has attracted a lot of interest because of its special properties such as its relatively narrow band gap and nontoxicity. This metal free polymer shows hydrogen production under visible light irradiation with high stability. However, its conversion efficiency is lower than TiO_2 or CdS and so further efforts need to be done in order to increase its efficiency. We will discuss different structures and compositions of these photocatalysts in details, which shows hydrogen activity under visible light irradiation.

3.3. Titanium dioxide based nanocomposites

Titanium dioxide has typically three crystal phases: anatase, rutile and brookite, among which anatase exhibits both high stability and high photocatalytic activity. The crystal structure of anatase and rutile are tetragonal, however brookite is orthorhombic.[56, 57] Various forms of TiO_2 have slightly different band gaps of around 3 eV, due to the variety of the crystal structures. Rutile is the thermodynamically stable form, and brookite does not usually show appreciable photocatalytic activity, but anatase is often indicated as the most active phase. The conduction band of TiO_2 is slightly higher than the reduction potential of water and so it can reduce protons when it is excited by light.

Some researchers synthesized nanocomposites of TiO_2 and some metal oxides which are activated in visible light region.[58-66] Interestingly, some of them showed higher hydrogen production in comparison with pristine TiO_2 due to visible light absorption and better charge separation. For instance, Martha et al. tried to increase hydrogen production by combining doped TiO_2 with V_2O_5.[61] Although N, S doped TiO_2 has a very low hydrogen evolution, the combination of the doped-TiO_2 with V_2O_5 exhibited 7 times higher hydrogen production under visible light irradiation (296.6 μmol h^{-1}). Xie et al. showed that nanocomposite of TiO_2/$BiVO_4$ had a much longer lifetime of

photoexcited charge carriers and so higher charge separation.[65] The main reason for this phenomenon is related to high movements of photoexcited electrons from $BiVO_4$ to TiO_2. Due to this reason, this photocatalyst had unexpected visible light activity for water splitting rather than $BiVO_4$ which was almost inactive in this region. They reported that $TiO_2/BiVO_4$ with molar ratio of 5%, could evolve 2.2 mol h^{-1} hydrogen, which was much higher than mixing with reduced graphene oxide nanosheet (0.75 mol h^{-1}) under the similar conditions.[66] Another group deposited Fe-TiO_2 nanoparticles (FTO) on the surface of $CaIn_2O_4$ nanorods (CIO).[63] This nanocomposite revealed hydrogen production in the presence of KI as sacrificial agent and Pt as the cocatalyst. The contact of these two nanoparticles facilitated charge separation and lead to higher hydrogen evolution. This nanocomposite exhibited H_2 production at a rate of 280 μmol h^{-1} g^{-1}, which was 12.3 and 2.2 times higher than $CaIn_2O_4$ and Fe-TiO_2, respectively. Due to the synthesis method (physical mixing of FTO and CIO), there is no control to have a uniform dispersion of FTO on CIO. In addition, the cocatalyst should be deposited on FTO in order to be more effective for hydrogen production. It seems that by applying some coating methods, the activity of this nanocomposite can improve, even more than 280 μmol h^{-1} g^{-1}.

It is worth mentioning that iron oxide is capable of using as metal organic framework (MOF) in diverse morphologies with titanium oxide.[67-69] For instance, Lin's group created a nanocomposite of mixed metal oxide (Fe_2O_3 and TiO_2) via metal organic frameworks (MOF) templates.[67] They used MIL-101 MOF (Fe source) to deposit amorphous TiO_2 and after deposition, they calcined the mixture in order to acquire the nanocomposite of Fe_2O_3/TiO_2. As a result, crystalline octahedral nano-shells were obtained which could produce hydrogen under visible light irradiation. Although TiO_2 can only activate under UV light and Fe_2O_3 has a more positive conduction band than reduction potential of H_2, this novel nanocomposite with a help of Pt metal as a cocatalyst produced 30.0 μmol g^{-1} of hydrogen in 48 hours in the presence of TEA as a sacrificial agent. The reason for this weird activity is that some iron ions from MIL-101 can be doped into TiO_2 crystallinity during the calcination process and the other converted into Fe_2O_3. Fe_2TiO_5 and Ti-doped Fe_2O_3 are both considered as activated photocatalysts under visible light in H_2 formation because of their small band gaps (Fe_2TiO_5 = 2.2 eV and Ti-doped Fe_2O_3 = 2.1 eV) and their edge of conduction bands which are more negative than H^+ reduction.[68] Moreover, further characterizations showed that this material was stable during hydrogen evolution and no decreasing in activity was observed. By introducing this kind of hollow nanostructure, the surface area of the photocatalyst increase significantly that results in higher activity owing to more available active sites. Another example of this type was developed in our group. We proposed a new route to prepare a novel type of photocatalytic hollow Fe_2O_3-TiO_2 nanostructure using MOF-UMCs as a hard template.[69] In this type of MOF-UMCs materials, each trimeric Fe(III) center possesses terminal water molecules that can be removed by vacuum and temperature treatments to generate Lewis acid sites, to which the amine group of titanium precursor can be grafted via the lone electron pair of nitrogen atom for the preparation of core/titania shell nanostructure, as illustrated in Figure 8. This achieved hollow nanostructure of Fe_2O_3–TiO_2–PtO_x photocatalyst possesses two distinct cocatalysts which are deposited separately on two sides of its hollow surface. The distance of two cocatalysts (wall thickness of template) was 15-35 nm that strongly facilitated charge separation and so increased photocatalytic activity. One of the cocatalyst was created from metal clusters of the MOF after calcination, located inside the hollow structure and the other was made from metal doping (PtO_x) on the surface of this nanocomposite. Interestingly, the visible light absorption band edge extended to 610 nm. Under visible light illumination and in the presence of lactic acid, this nanocomposite could produce 22 μmol h^{-1} hydrogen without any reduction in its activity even after 5 cycles. The total amount of H_2 after five cycles was 110 μmol under visible light irradiation. Although this amount of hydrogen production was not so much in comparison with other photocatalysts, but this approach may be used to develop other hollow structures with higher activity for hydrogen evolution in visible light region.

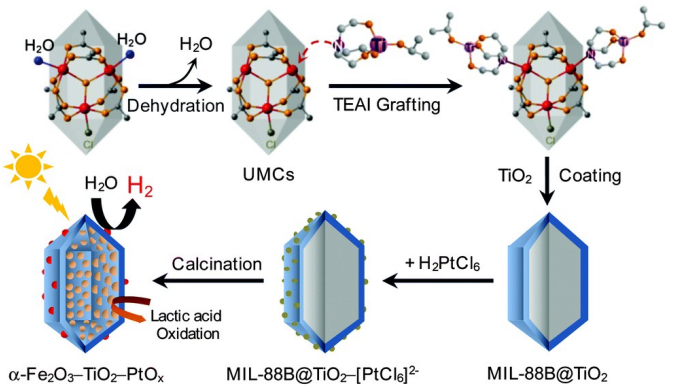

Figure 8: Schematic illustration of the formation of the hollow Fe_2O_3–TiO_2–PtO_x nanocomposite.[69]

In addition to metal oxides, scientists tried to mix diverse metal sulfides with titanium oxide due to their higher visible light absorption. CdS is the best metal sulfides to combine with TiO_2 because of its proper conduction band and higher efficiency. Due to the importance of this kind of nanocomposite, different compositions and morphologies will be discussed thoroughly in another section. Here, other metal sulfides composites with TiO_2 are explained in detail.[70-74] It was reported that the single nanoparticles of In_2S_3 or Pt/TiO_2 were not active in the H_2 formation under visible light irradiation. However, the combined In_2S_3/Pt/TiO_2 nanostructure produced H_2 under visible light at the rate of 135 μmol h^{-1} with the 1% quantum yield at $\lambda \geq 420$ nm.[71] In this nanocomposite, both Pt/TiO_2 and In_2S_3 nanoparticles were in close contact by embedding Pt/TiO_2 nanoparticles in the interstices of the In_2S_3. The optimum ratio of In_2S_3/Pt/TiO_2 was reported to be 3:2. Furthermore, Jang et al. synthesized a photocatalyst composite of titanium dioxide and $AgGaS_2$ with solid state reaction followed by sol-gel method.[74] In the presence of sulfide and sulfite solution and Pt as a cocatalyst, this composite showed a very good activity for hydrogen under visible light irradiation. Due to the conduction band structure, excited electrons can transfer from $AgGaS_2$ to TiO_2 and from there they can react with protons to produce hydrogen. The maximum quantum yield was 17.5% for the optimum ratio of 1:2 (TiO_2:$AgGaS_2$) and 1% Pt.

Some researchers synthesized nanocomposites of TiO_2 with different carbon based materials such as carbon coated metal[75], carbon quantum dots[76, 77], carbon nanotube[78] and graphene.[79-82] For example, Peng's group synthesized a novel nanocomposite of carbon coated Ni (denoted as Ni@C) and TiO_2.[75] This nanocomposite consists of nanorods with 10 nm in diameter and 40-100 nm in length. By using triethanolamine as a

sacrificial reagent, this nanostructure could produce hydrogen under visible light irradiation. The highest activity was obtained when 5% of Ni was used in this nanocomposite (300 μmol h^{-1}). Furthermore, the apparent quantum yields are 12% and 7% for λ > 420 and λ > 520 nm, respectively. These yields were much higher than the same for neat Ni@C without TiO_2. Table 1 shows some nanocomposites of titanium dioxide as well as their activity under visible light irradiation.

Table 1: Different nanocomposites of TiO_2 active for hydrogen production (λ>420 nm).

Semiconductor 1	Semiconductor 2	Cocatalyst	Sacrificial reagent	Light Source	Hydrogen production (μmol h^{-1} g^{-1})	Quantum yield (%)	Refs
TiO_2	Carbon coated Ni (Ni@C)	---	Triethanolamine	300 W Xe, λ ≥ 420 nm	2000	12 at λ=420 nm 7 at λ=520 nm	75
TiO_2 nanosheet	Graphene	---	Methanol	350 W Xe	736	No data	79
TiO_2	In_2S_3	Pt	Na_2S/Na_2SO_3	300 W Xe, λ ≥ 420 nm	1350	1 at λ=420 nm	71
TiO_2 mesocrystals	Au nanoparticles	Pt	Propanol	Xe light, λ > 460 nm	0.5	No data	83
N,S doped TiO_2	V_2O_5	Pt	Methanol	125 W Hg, λ ≥ 400 nm	2966	No data	61
TiO_2	MOF MIL 101	Pt	Triethanolamine	450 W Xe, λ ≥ 420 nm	1250	No data	67
TiO_2	MOF MIL 88	PtO_x	Lactic acid	300 W Xe, λ ≥ 420 nm	1100	No data	84
TiO_2	$AgIn_5S_8$	Pt	Na_2S/Na_2SO_3	300 W Xe, λ ≥ 420 nm	850	No data	73
mesoporous TiO_2	WS_2	Pt	Na_2S	350 W Xe, λ > 430 nm	200	No data	85
P25	Carbon quantum dot (CQD)	---	Methanol	500 W Halogen, λ > 450 nm	10	No data	77
$AgGaS_2$	TiO_2	Pt	Na_2S/Na_2SO_3	450 W Hg, λ ≥ 420 nm	4200	17.5 at λ=420 nm	74
$CaIn_2O_4$	Fe-TiO_2	Pt	KI	300 W Xe, λ ≥ 420 nm	280	No data	63
Graphene	Au–TiO_2	---	Methanol	3W LED, λ=420 nm	296	4.1 at λ=420 nm	80
Fe_2O_3	TiO_2	---	Na_2S/Na_2SO_3	300 W Xe, λ ≥ 420 nm	7253	0.94 at λ=447 nm	64

3.4. CdS based nanocomposite

CdS is one of the best semiconductors for photocatalytic hydrogen production because of its narrow band gap and conduction edge-band position. In other words, it can absorb visible light with long wavelength and also it can reduce protons to hydrogen. However, this photocatalyst has two main disadvantages which are: (1) due to its small band gap, the recombination process of photoexcited electrons and holes are very easy; (2) this semiconductor is unstable under light irradiation and it is effortlessly corroded by excited holes. For these reasons, CdS needs to combine with other semiconductors in order to overcome its drawbacks.

Due to a highly visible light absorption of CdS (2.42 eV), scientists tried to enhance photocatalytic efficiencies of CdS with modifying nanostructures of this semiconductor. Nanostructure of CdS provided more active sites for water splitting reaction and so increase its photocatalytic activity.[86] Another technique is preparing CdS in nano-porous structures that can raise the quantum yield up to 60% in the presence of Na_2SO_3 and Na_2S as sacrificial agents (λ ≥ 420 nm).[87] The main reasons for this development in quantum yield are effective charge separation, fast movements of charge carriers, and quick chemical reaction at the interface of CdS nanostructure. Combing CdS nanoparticles with another semiconductor is another way to enhance its photocatalytic efficiency.[88]

Although metal oxides are usually possess wide band gap and cannot absorb long wavelength of sunlight spectrum, they are very stable during photocatalytic processes. Therefore, some studies were done in order to mix these semiconductors together and obtained more efficient photocatalysts.[55, 89-99] For instance, Wang and co-workers prepared core-shell nanostructures from ZnO and CdS.[89] This nanocomposite was able to split water to produce H_2 with sacrificial reagents. Interestingly, loading RuO_2 cocatalyst showed more activity rather than Pt metal. In addition, the ratio of ZnO to CdS in $(ZnO)_{1-x}(CdS)_x$, strongly affected its photocatalytic efficiency and it slightly dropped by raising CdS molar ratio. The highest H_2 evolution is 2.96 mmol h^{-1} g^{-1} by x = 0.2, which is 34.4 times and 7.8 times higher than that of ZnO nanorods (prepared by the hydrothermal route) and CdS (prepared by the solid state route), respectively. As mentioned before, RuO_2 has a great impact on photocatalytic activity resulted in a sudden increase by around 200%. This nanocomposite could constantly produce H_2 for more than 30 h. Hou et al. synthesized a nanocomposite of CdS (2.45 eV) and TaON (2.5 eV) in a core-shell structure.[91] They deposited TaON on the core of CdS and used Pt as a cocatalyst. Due to the band edge positions of these semiconductors, electrons migrate from CdS to TaON and holes can move from TaON to CdS. Although hydrogen evolution rates for pure CdS and TaON were 13.5 and 9 μmol h^{-1}, respectively, this nanocomposite could evolve 306 μmol h^{-1} hydrogen using a sacrificial reagent. Moreover, combining this nanostructure with 1wt% graphene oxide led to produce more than two times higher hydrogens than the previous one with a 31% quantum yield under visible light irradiation. Nonetheless, they didn't examine the stability of this nanocomposite for multiple cycles in longer runtime. One of the purposes of combining CdS with other materials is to enhance its stability during reaction time. Usually the photocatalyst should run multiple cycles of hydrogen production in order to observe its stability under light illumination.

In addition to binary metal oxides, some researchers made a nanocomposite of CdS and ternary metal oxides.[100-103,110,111] In these nanostructures, generated holes can transfer from CdS to metal oxides, due to their valence band positions, and photoexcited electrons remain in the conduction band of CdS and reduce protons to hydrogen. These charge carriers' movements are completely different than in other nanocomposites. Usually electrons transfer to other semiconductors from CdS, but in this case holes transfer and so both charge recombination and photocorrosion are avoided. However, it should be noted that the synthesis procedure of these ternary nanocomposites is usually complicated and needs careful attention in order to obtain desired nanostructure.

Furthermore, CdS can be combined with other metal sulfides in various morphologies such as nanocrystals[104], nanowires[105], nano-layers[106] in order to enhance its efficiency. Among all metal sulfides, ZnS attracts more attention due to its high ability to form solid solution with CdS which results in higher charge separation and more quantum efficiency.[107-114] For

example, a solid solution of $(Zn_{0.95}Cu_{0.05})_{1-x}Cd_xS$ was examined with various ratios of Cd for H_2 production under visible light and in the presence of SO_3^{2-} and S_2^{2-}.[107] This solid solution consisted of nanocrystals of about 2-5 nm and had a band gap of 2.0 eV. This nanostructure showed 508 μmol h^{-1} without any cocatalyst and possesses a quantum yield of 15.7% under visible light when x equal to 0.33. However, by depositing 0.75% Pt, its activity enhanced significantly and hydrogen production and quantum yield reached to 1.09 mmol h^{-1} and 31.8%, respectively. Moreover, this nanocomposite was stable after 3 cycles 12 h. Zhang and al. synthesized a nanocrystal of solid solution ZnS-CdS that was involved in H_2 evolution at 420 nm.[109] They used MoS_2 compound as a cocatalysts and reported that with 0.2 wt% of this cocatalysts, the hydrogen formation was 36 times higher than CdS with noble metals as cocatalysts.[115, 116] Moreover, Liu et al. showed that nano-twin structures of $Cd_{1-x}Zn_xS$ solid solution could produce hydrogen from water without noble metals. Its apparent quantum yield was reported to be 43% at 425 nm in the presence of sacrificial reagents.[110] Another type of nanocomposites of ZnS and CdS is the physical mixture of their nanoparticles without making a solid solution phase. Shen et al. improved nanocrystals of ZnS/CdS (5-10 nm) with In_2S_3 without any surfactant or supports at room temperature and normal pressure.[104] These microspheres could produce hydrogen from aqueous solution of sulfide and sulfite ions with no cocatalysts and it was reported that the quantum yield achieved to 40.9 % at $\lambda \geq 420$nm. The optimum ratio of CdS is 75%, which can produce 8.1 mmol h^{-1} g^{-1} hydrogen. Despite the fact that this nanocomposite showed a very high hydrogen evolution, no further experiments were done to examine its stability during hydrogen production, which should be considered in further studies.

In addition to solid solution, CdS can mix with other metal sulfides in order to increase hydrogen production under visible light irradiation.[105, 117-119] For instance, TiS_2 and TaS_2 are both semiconductors with small band gap less than 1 eV. A nano-layer combination of one of these two semiconductors with nanoparticles of CdS resulted in high efficient photocatalysts for H_2 evolution from an aqueous solution of benzyl alcohol.[106] The nanocomposite of TiS_2 and CdS could generate 1000 μmol $h^{-1}g^{-1}$ hydrogen, whereas the other one (TaS_2 and CdS) showed 2.3 times higher hydrogen evolution (2320 μmol $h^{-1}g^{-1}$) under visible light irradiation. The reason for this phenomenon was explained by the metallic nature of few-layer TaS_2. In another study, Zhang et al. deposited NiS nanoparticles on the CdS surface with the help of hydrothermal route.[117] They reported that the nanocomposite with 1.2% of NiS had the highest activity and quantum yield. Its quantum efficiency under visible light irradiation (λ > 420nm) was 51.3 %, which was the highest photocatalyst activity without noble metal cocatalyst. In addition, its H_2 evolution rate was 2.18 mmol h^{-1} which was 35 times higher than that of alone CdS. Hou et al. decoreated $CdLa_2S_4$ microspheres with CdS nanocrystals by a hydrothermal procedure in order to enhance hydrogen generation.[114] Due to the intimate contact of these nanoparticles and also high dispersion of CdS nanocrystals, this nanocomposite exhibited a significant quantum yield of 54% under visible light region corresponding to 2250 μmol h^{-1} g^{-1}, which was 9 times higher than the pristine $CdLa_2S_4$.

Carbon nanotubes is one of the most famous building block for synthesizing nanostructures that can be combine with diverse semiconductors particularly CdS in order to enhance charge separation step, as demonstrated in Figure 9.[120-125] Furthermore, graphene nanosheet has some special properties such as high surface area, high charge carrier mobility (due to its two-dimensional sp^2-hybridized), and good mechanical stability.[126] The intimate contact between CdS and graphene can enhance the migration of photoexcited electrons and surpass the recombination process more efficiently. In principle, photoexcited electrons move from the conduction band of the CdS to graphene and according to great mobility of electrons on the graphene sheets, the recombination process is partially prevented.[123, 125, 127-133] For instance, Li et al. synthesized CdS nanoparticles of about 3 nm in autoclave and they dispersed them on graphene nanosheet completely.[133] This nanocomposite, which had 1 wt% graphene and 0.5 wt% Pt, showed 1.12 mmol h^{-1} hydrogen evolution from a solution of lactic acid. This rate of hydrogen production was around 5 times higher than pristine CdS and the apparent quantum efficiency was reported 22.5% at $\lambda \geq 420$ nm.

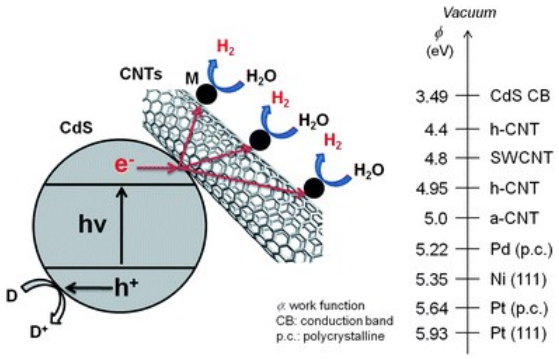

Figure 9: Illustration of photocatalytic hydrogen production in CdS/CNT/M suspensions under light irradiation. M and D refer to metal catalyst and electron donor, respectively. On the right-hand side, the reported work functions of selected materials are given. [121]

There have been different methods to synthesize graphene-based photocatalysts, but the simplest and most direct technique is to mix graphene with target semiconductors.[134-136] The other popular method to provide nanocomposites of various semiconductors with graphene is in situ growth method in which graphene oxide (GO)[91, 133, 137] or reduced graphene oxide (RGO)[138-146] is chosen as starting materials.[147] Nanocrystals of CdS or other semiconductors can grow on the surface of graphene nanosheet via oxygen-containing functional groups which act as nucleation sites.[148] The structure and electrical properties of RGO as well as the location of the conduction band of CdS and RGO lead the photoexcited electrons transfer from CdS to RGO and from there, they can reduce hydrogen atoms (Figure 10).

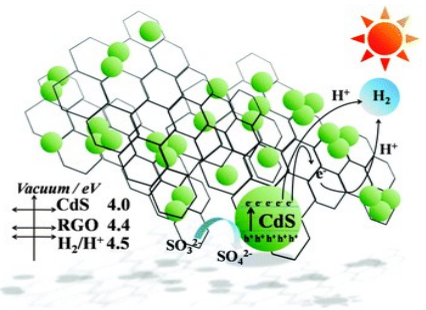

Figure 10: Schematic diagram of the proposed mechanism for photocatalytic H_2 production over RGO–CdS.[146]

Table 2: Various nanocomposites of CdS active under visible light illumination.

Semiconductor 1	Semiconductor 2	Cocatalyst	Sacrificial reagent	Light source	Hydrogen production (μmol h^{-1} g^{-1})	Quantum yield (%)	Refs
CdS	SrS	---	Na_2S/Na_2SO_3	300 W Xe, λ > 400 nm	246	10 at λ = 420 nm	105
CdS	ZnCu	--- Pt	Na_2S/Na_2SO_3	300 W Halogen, λ ≥ 420 nm	1693 3633	15.7 at λ = 420 nm 31.8 at λ = 420 nm	109
CdS	CuIn	--- Pt	Na_2S/Na_2SO_3	300 W Xe, λ ≥ 420 nm	649.9 2456	2.14 at λ = 420 nm 26.5 at λ = 420 nm	108
CdS	ZnO	Pt	Na_2S/Na_2SO_3	300 W Xe	2960	No data	89
CdS nanorods	CdSe	Pt	2-propanol	300 W Xe	40500	20 at λ = 450 nm	149
CdS	Ni/NiO/$KNbO_3$	---	Isopropanol	500 W Hg−Xe, λ > 400 nm	203.5	8.8 at λ > 400 nm	103
CdS	Ni/NiO/$KNbO_3$	---	Isopropanol	500 W Hg−Xe, λ > 400 nm	150	4.4 at λ > 400 nm	102
CdS	$LaMnO_3$	---	Na_2S/Na_2SO_3	300 W Xe, λ ≥ 420 nm	595	No data	101, 150
$Cd_{0.8}Zn_{0.2}S$	ZnO	Pt	benzyl alcohol	450 W Xe,	36500	50.4 at λ = 400 nm	113
CdS nanorods	NiS	---	Na_2S/Na_2SO_3	300 W Xe, λ ≥ 420 nm	1131	6.1 at λ = 420 nm	151
$Cd_{0.1}Zn_{0.9}S$	Multi-walled carbon nanotube	---	Na_2S/Na_2SO_3	300 W Xe, λ ≥ 420 nm	1563.2	7.9 at λ = 420 nm	122
CdS	CeO_2	---	Na_2S/Na_2SO_3	300 W Xe	223	No data	93
CdS	Multi-walled carbon nanotubes	Pt	Na_2S/Na_2SO_3	300 W Halogen, λ > 400 nm	825	No data	121
CdS	MWCNTs	---	Na_2S/Na_2SO_3	300 W Xe, λ ≥ 420 nm	4977	2.16 at λ = 420 nm	120
CdS	ZnS	Ru	Formic acid	300 W Xe, λ ≥ 420 nm	6000	20 at λ = 400 nm	152
In_2S_3	CdS-ZnS	---	Na_2S/Na_2SO_3	300 W Xe, λ > 400 nm	8100	40.9 at λ = 420 nm	104
$CdLa_2S_4$ microspheres	CdS nanocrystal	Pt	Na_2S/Na_2SO_3	300 W Xe, λ ≥ 420 nm	2250	54 at λ = 420 nm	114
ZnS	CdS	---	Na_2S/Na_2SO_3	500 W Halogen	46	No data	112
TaON Graphene oxide	CdS CdS@TaON	Pt	Na_2S/Na_2SO_3	300 W Xe, λ ≥ 420 nm	1530 3165	15 at λ = 400 nm 31 at λ = 420 nm	91
ZnO	CdS	---	Na_2S/Na_2SO_3	500 W Xe, λ > 400 nm	851	3 at λ = 420 nm	94
$CdOW_4$	CdS	---	Na_2S/Na_2SO_3	500 W Xe	90.25	No data	100
reduced graphene oxide nanosized	CdS	MoS_2	lactic acid	350 W Xe, λ ≥ 420 nm	1980	9.8 at λ = 420 nm	142
MoS_2/graphene hybrid	CdS	MoS_2	lactic acid	300 W Xe, λ ≥ 420 nm	9000	28.1 at λ = 420 nm	131
reduced graphene oxide	UiO-66 and CdS	Pt	Na_2S/Na_2SO_3	300 W Xe, λ >400 nm	2100	No data	141
vermiculite	CdS quantum dot		Na_2S/Na_2SO_3	300 W Xe, λ ≥ 420 nm	920	17.7 at λ = 420 nm	153
SiC	CdS particles	Pt	Na_2S/Na_2SO_3	300 W Xe, λ ≥ 420 nm	555	0.2 at λ = 420 nm	154
framework of structured WO3	orderly depositing Au and CdS	---	Na_2S/Na_2SO_3	300 W Xe, λ ≥ 420 nm	1730	No data	95
ZSM-5 type metalosilicates	CdS nanoparticles	---	Na_2S/Na_2SO_3	500 W Osram, λ ≥ 420 nm	11000	65.62 at λ = 420 nm	155
γ-TaON hollow spheres	CdS nanoparticles	MoS_2	Na_2S/Na_2SO_3	300 W Xe, λ ≥ 420 nm	3142.5	No data	96
ZnO core/shell nanofibers	CdS	---	Na_2S/Na_2SO_3	500 W Xe, λ ≥ 420 nm	354	No data	97
$ZnIn_2S_4$ heterostructures coupled with graphene	CdS quantum dots	Pt	Na_2S/Na_2SO_3	300 W Xe, λ ≥ 420 nm	27000	56 at λ = 420 nm	132
Carbon nanotube	$Zn_xCd_{1-x}S$	---	Na_2S/Na_2SO_3	500 W Xe	6030	No data	123
Carbon nanotube	CdS	NiS	Na_2S/Na_2SO_3	350 W Xe, λ ≥ 420 nm	12130	No data	124
reduced graphene oxide	$Cu_{0.02}In_{0.3}ZnS_{1.47}$	Pt	Na_2S/Na_2SO_3	800 W Xe–Hg, λ ≥ 420 nm	3800	No data	140
Ti-MCM-48 mesoporous	CdS	RuO_2	Ethanol	300 W Xe, λ > 400 nm	2730	36.3 at λ = 400 nm	156
MoO_3	CdS	---	Na_2S/Na_2SO_3	300 W Xe, λ ≥ 420 nm	5250	28.86 at λ = 420 nm	98

Table 2. Continue

Semiconductor 1	Semiconductor 2	Cocatalyst	Sacrificial reagent	Light source	Hydrogen production (μmol h^{-1} g^{-1})	Quantum yield (%)	Refs
cubic MCM-48 mesoporous	CdS	Pt	Ethanol	300 W Xe, λ > 400 nm	1810	16.6 at λ = 400 nm	157
Reduced graphene oxide	CdS	---	Na_2S/Na_2SO_3	300 W Xe, λ ≥ 420 nm	4200	10.4 at λ = 420 nm	139
Ga_2O_3	CdS quantum dots	Pt	Lactic acid	300 W Xe, λ ≥ 420 nm	9052	43.6 at λ = 460 nm	99
In_2O_3					9382	45.3 at λ = 460 nm	
TiS2	CdS	---	Benzyl alcohol	450 W Xe, λ > 400 nm	1000	No data	106
TaS2					2320		
MCM-41	CdS	---	Triethanolamine	300 W Xe, λ ≥ 430 nm	47.1	No data	158
$AgGaS_2$	CdS	Pt	Na_2S/Na_2SO_3	450 W Hg, λ ≥ 420 nm	4730	19.7at λ = 420 nm	159
reduced graphene oxide	CdS	$Ni(OH)_2$	Na_2S/Na_2SO_3	300 W Xe, λ ≥ 420 nm	4731	No data	138
graphene oxide	CdS	---	Na_2S/Na_2SO_3	300 W Xe, λ ≥ 420 nm	3410	4.8at λ = 420 nm	137
graphene oxide	CdS clusters	Pt	lactic acid	350 W Xe, λ ≥ 420 nm	5600	22.5at λ = 420 nm	133
N-graphene	CdS	---	Na_2S/Na_2SO_3	300 W Xe, λ ≥ 420 nm	1050	No data	130
g-C_3N_4	CdS quantum dots	Pt	Methanol	300 W Xe, λ ≥ 420 nm	348	No data	160

Table 2 summarized hydrogen production of different nanocomposite of CdS under visible light irradiation with their quantum yields.

3.5. CdS and TiO_2 nanostructure

TiO_2 and CdS are the most studied semiconductors during the last decades due to their photocatalytic properties and benefits. However, each of them has some drawbacks that limit their applications for hydrogen production from sunlight. For example, TiO_2 has a wide band gap inapplicable for visible light absorption and CdS is instable during photocatalytic reactions. The combination of these semiconductors in nanoscale leads to have more efficient photocatalysts that can generate hydrogen under visible light irradiation with high stability. Under visible light illumination, CdS can absorb photons and produce holes and electrons. Although TiO_2 cannot absorb visible light, due to its wide band gap, excited electrons can move from CdS to TiO_2. This leads to the better charge separation, and results in higher quantum yield. It should be noted that the excited holes remain in the valence band of CdS and from there; they can oxidize any sacrificial agents. [161, 162] Various nanocomposites with different morphologies can be created form CdS and TiO_2, as shown in Table 3. Some important morphologies will be discussed here, which results in higher light absorption and higher hydrogen evolution in visible light region.

Generally, two different morphologies for mixing CdS nanoparticles and titanate nanotubes have been proposed in order to improve photocatalytic activity, as illustrated in Figure 11.[163-168] CdS/titanate nanotubes (CdS/TNTs) were reported to have higher increase in photocatalytic activity in comparison with traditional nanocomposite CdS@TNTs.[163] The CdS/TNTs nanostructures lead to have a proper dispersion of CdS as well as intimate multipoint contacts between two nanocrystals. It is clear that the ratio of Cd/Ti plays an important role in photocatalyst activity. The optimum value of this proportion was 0.05, which corresponds to 6 wt% of CdS in photocatalysts. With the optimum cocatalyst quantity of Pt (2.0 wt%), the CdS/TNTs could generate 353.4 μmol h^{-1} hydrogen with 25.5% quantum yield under visible light. Nevertheless, the quantum yield of traditional CdS@TNTs could hardly reach 2.7% and as mentioned before, changing the structure of nanoparticles can have major impacts on their activity. It is noteworthy that this nanocomposite was stable for hydrogen production during 120 hr of 6 cycles. Therefore, this nanostructure improved noticeably the stability of photocatalyst during hydrogen evolution .

Many researchers have investigated the deposition of CdS nanoparticles inside different nanostructure of titanate such as tubular and nanotubes with the aim of obtaining high efficient nanocomposites.[164, 169] Li et al. deposited homogeneously CdS nanoparticles inside the TiO_2 nanotubes.[164] They examined its photocatalytic water splitting with electron donors containing S^{2-}, SO_3^{2-} at wavelength of 420 nm. They attained 43.4% quantum yield for H2 evolution. This is due to the quantum size effect of CdS nanoparticles as well as synergetic effects between two nanocomposites. This also means that the potential energy at the interface of CdS and TiO_2 would help electrons to transfer from CdS to TiO_2 more easily and consequently enhanced photocatalytic activity.

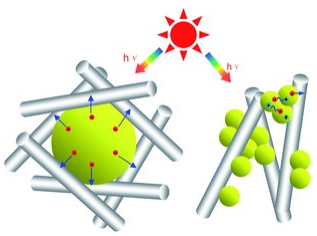

Figure 11: Schematic illustration of the two different architectures in CdS/TNTs (left) and CdS@TNTs (right).[163]

CdS nanoparticles can also be deposited on nanosheets of titanate that leads to increase quantum yield of nanocomposite.[170-174] The powerful interaction between titanate 2D nanostructures and CdS helped to create visible light absorption photocatalysts with high stability towards photocorrosion of CdS. Our group synthesized an ultrathin titanate nanodisks (TNDs) by the solvothermal method.[175] After that, they grew both CdS nanoparticles as a visible light semiconductor and Ni nanoparticles as a cocatalyst on the surface of TNDs for hydrogen evolution. This nanocomposite was able to separate photoexcited charges efficiently and as a result it showed a very high activity for water splitting under visible light irradiation.

The concept of depositing a cocatalyst on the other surface (here on TNDs), would help to enhanced photocatalytic activity by increasing charge separation and preventing recombination phenomena. As can be seen in Figure 12(a), excited electron can easily transfer from CdS to TNDs and from there to Ni cocatalyst [170]. With an optimum ratio of CdS/TNDs and Ni loading, this nanocomposite can generate H_2 from water-methanol solution under visible light irradiation. The hydrogen evolution rate was 15.326 mmol g^{-1} h^{-1} during 15 h of reaction, which results in having 24% quantum yield at $\lambda \geq 420$ nm. It is noteworthy that this approach of mixing semiconductor with TND can also be used for other efficient visible light active semiconductor. The intimate contact between TND and CdS play a crucial role in this kind of nanostructure. In other word, physical mixing of these semiconductors cannot result in high photocatalytic activity. By growing CdS as well as selective deposition of Ni clusters on the surface of TND by means of ion exchange method, we were certain that nanoparticles had intimate contact and so charge carriers can easily transfer between semiconductors, as shown in Figure 12 (b).[176]

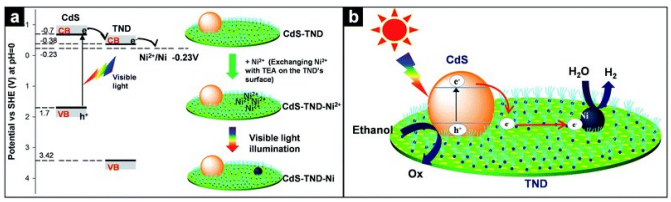

Figure 12: Schematic illustration of the electron transfer in the photoreduction of Ni^{2+} adsorbed on the surface of TNDs under visible light illumination and schematic illustration of the formation of Ni clusters on the surface of TND by visible-TND composites by visible light illumination (a). Schematic illustration of the charge transfer in CdS-TND-Ni MPs in the photocatalytic H_2 production from water-ethanol solution under visible light (b).[170]

Table 3: Different nanocomposites of CdS and TiO_2

Semiconductor 1	Semiconductor 2	Cocatalyst	Sacrificial reagent	Light source	Hydrogen production (μmol h^{-1} g^{-1})	Quantum yield (%)	Refs
$Na_2Ti_2O_4(OH)_2$ nanotube	CdS	Pt	Na_2S/Na_2SO_3	350 W Xe, $\lambda \geq 430$ nm	545	2.7 at $\lambda = 430$ nm	167
TiO_2 nanotubes	CdS	Pt	Na_2S/Na_2SO_3	300 W Xe, $\lambda \geq 420$ nm	2680	43.3 at $\lambda = 420$ nm	164
Titanate nanotubes	CdS	Pt	Na_2S/Na_2SO_3	500 W Xe, $\lambda \geq 430$ nm	1767	25.5 at $\lambda = 420$ nm	163
Titanate nanodisks	CdS	Ni	Ethanol	300 W Xe, $\lambda \geq 420$ nm	11038	21 at $\lambda = 420$ nm	175
Titanate nanodisks	CdS	Ni	Ethanol	300 W Xe, $\lambda \geq 420$ nm	15326	24 at $\lambda = 420$ nm	170
TiO_2 nanosheet	CdS nanoparticles	---	Na_2S/Na_2SO_3	350 W Xe, $\lambda \geq 400$ nm	1651	8.9 at $\lambda = 420$ nm	171
TiO_2	CdS	Pt	Na_2S/Na_2SO_3	450 W Xe, $\lambda \geq 420$ nm	4848	No data	177
TiO_2	Hexagonal CdS	---	Na_2S/Na_2SO_3	500 W Osram	8990	No data	178
TiO_2 nanorods	CdS nanoparticles	Ni	Ethanol	300 W Xe, $\lambda \geq 420$ nm	33.63	No data	168
Titanate nanotubes	$Cd_{0.5}Zn_{0.5}S$	---	Na_2S/Na_2SO_3	500 W Xe, $\lambda \geq 430$ nm	1738.5	38.1 at $\lambda = 420$ nm	179
TiO_2 nanosheet	CdS NPs	Pt	Lactic acid	350 W Xe, $\lambda \geq 420$ nm	6625	13.9 at $\lambda = 420$ nm	172
TiO_2	CdS	Pt	Na_2S/Na_2SO_3	350 W Xe, $\lambda \geq 420$ nm	6720	4.5 at $\lambda = 420$ nm	180
Titanate spheres	CdS nanoparticles	---	Na_2S/Na_2SO_3	300 W Xe, $\lambda \geq 420$ nm	75	No data	181
sub-nanometer-thick layered titanate nanosheet	CdS quantum dots (QDs)	---	Na_2S/Na_2SO_3	300 W Xe, $\lambda \geq 420$ nm	1000	No data	173
Bulk CdS	TiO_2 nanoparticles	Pt	Na_2S/Na_2SO_3	350 W Xe, $\lambda \geq 420$ nm	6400	No data	161
hex-CdS TiO_2	TiO_2 CdS	Pt	glycerol	300 W Xe, $\lambda \geq 420$ nm	22 65	No data	182
CdS nanowires	TiO_2 nanoparticles	Pt	Na_2S/Na_2SO_3	500 W Xe, $\lambda \geq 420$ nm	110	No data	183
CdS bulk	TiO_2 nanoparticles	Pt	Na_2S/Na_2SO_3	350 W Xe, $\lambda \geq 420$ nm	4224	No data	184
Chromosilicate	CdS–TiO_2	---	Na_2S/Na_2SO_3	500 W Osram, , $\lambda \geq 420$ nm	2580	76.27at $\lambda = 450$ nm	185
TiO_2	CdS	Au	Na_2S/Na_2SO_3	300 W Xe, $\lambda \geq 420$ nm	1970	No data	186

In another technique, researchers tried to deposit TiO_2 nanoparticles on CdS nanostructures.[161, 162, 182-184, 186] In most of them, a cocatalyst should be utilized in order to have hydrogen production. For instance, Jang et al. made a nanocomposite of CdS nanowires with a high crystallinity, which had TiO_2 nanocrystals on their surfaces, as shown in Figure 13.[183] Under visible light, this nanostructure displayed hydrogen production from an aqueous solution of sulfide and sulfite ions. The optimum ratio of TiO_2 in this nanostructure would be 0.2, which led to having the highest activity under visible light irradiation. The possible role of TiO_2 NP is to provide sites for collecting the photoelectrons generated from CdS NW, enabling thereby an efficient electron-hole separation as depicted in Figure 13.

Preparing nanocomposite is a very delicate process and each step should be considered precisely, even though the nanostructure and crystallinity may change by order of adding precursors. Park et al. showed that reversing chemical precipitation order of CdS on TiO_2 nanoparticles caused to have different H_2 evolution rates in H_2 evolution under the same

conditions.[177] They prepared CdS_R by adding Cd^{2+} in aqueous solution containing S^{2-} and Pt-loaded TiO_2. Another nanocomposite with an equal molar ratio was prepared by adding sulfide drops into the solution of Cd^{2+} and Pt-TiO_2 (Cd_RS). Surprisingly, CdS_R showed 10 times higher hydrogen evolution than Cd_RS under visible light irradiation (Figure 14).

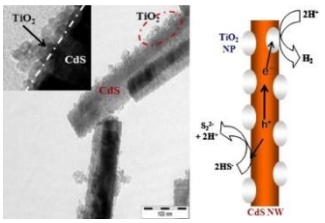

Figure 13: A nanocomposite consisting of CdS NW with high crystallinity decorated with nanosized TiO_2 NPs.[183]

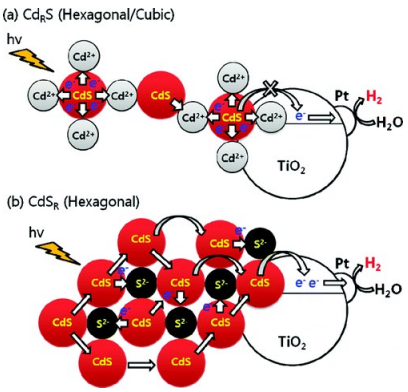

Figure 14: Schematic illustration for photocatalytic hydrogen production mechanisms of Cd_RS and CdS_R hybrids.[177]

Khatamian et al. prepared a metalosilicate-based (ferrisilicate and aluminosilicate) nanocomposite of CdS/TiO_2 via hydrothermal method.[178] Utilizing metalosilicate support has many advantages such as offering high surface area and providing homogenous dispersion of CdS nanoparticles. Moreover, this support both prevents agglomeration of the semiconductor and facilitates electron transfer and separation. It is noteworthy to consider that applying ferrisilicate, the presence of partially occupied d orbitals of Fe^{3+}, which can interact with TiO_2 orbitals, enhances the photocatalytic activity, while applying aluminosilicate as a support didn't improve its activity compared to unsupported composite. In the case of CdS phase, hexagonal structure showed around sixfold higher photocatalytic activity than cubic one.

Vu et al. provided nanocomposite of TiO_2 nanorods and CdS nanoparticles with Ni clusters in order to enhance charge separation and photocatalytic activity.[168] A dominant feature of this nanorod-based material is that nanoparticles of second semiconductors could be dispersed uniformly on the nanorod surface. Ni nanoparticles acting as cocatalysts were deposited on the surfaces of these nanorods selectively. This configuration can improve the efficiency of electron transfer from the sensitized CdS nanoparticles to TiO_2 and then to Ni clusters, as depicted in Figure 15. The H_2 production rate was 33.36 μmol h^{-1} g^{-1} under visible light in the presence of sacrificial reagent, which was about 44 times higher than neat Ni-CdS system.

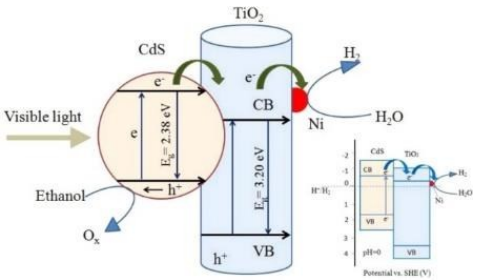

Figure 15: Mechanism illustration of the activity of Ni–TiO_2/CdS under visible light for the production of H_2; inset is the potential redox energy corresponding to CdS, TiO_2, and H^+/H_2.[168]

A new ternary nanostructure of three different nanoparticles was synthesized in order to enhance H_2 production under visible light irradiation.[186] Firstly, they synthesized nanoparticles of Au with an average size of 40 nm. After this step, they grew TiO_2 nanocrystal as a shell structure on the Au nanoparticles via hydrothermal method according to previous researches.[187] Then, they deposited CdS nanoparticles on the surface of Au@TiO_2 core–shell nanostructures. This ternary nanocomposite showed considerable high activity for H_2 evolution rather than both binary nanostructures (CdS−TiO_2 or Au@TiO_2). This ternary design builds up a transfer path for the photoexcited electrons of CdS to the core Au particles via the TiO_2 nanocrystal bridge and thus effectively suppresses the electron-hole recombination on the CdS photocatalyst. However, this nanocomposite is very complicated to obtain and needs precise conditions for each step of the synthesis, which is one of its drawbacks in comparison with other binary nanocomposites for hydrogen production.

3.6. g-C_3N_4 based nanocomposite

Graphitic carbon nitride (g-C_3N_4) is a metal-free semiconductor that consists of s-triazine or tri-s-triazine units. These units are connected in two-dimensional graphite-like framework by amino groups in each layer and weak van der Waals forces between layers.[188] As a result, this polymeric semiconductor shows very high thermal and chemical stability. In 2009, Wang et al. synthesized g-C_3N_4 from cyanamide by pyrolysis at high temperature (400-600 ºC).[189] The obtained semiconductor not only could produce hydrogen under visible light irradiation from aqueous solution of triethanolamine (TEA), but also it had steady hydrogen production rate over 75 hr. Since then, other researchers tried to synthesize g-C_3N_4 from other nitrogen rich precursors such as dicyanamide, urea and melamine.[190] In addition, some other scientists combined it with other semiconductors or charge carriers mediator to boost its photocatalyst activity.[191-196] Here, we discuss various heterojunctions of g-C_3N_4 and semiconductors that could improve hydrogen production under visible light (Table 4).

Due to the structure similarity of carbon bonds in carbon based nanostructures (nanotubes and graphene) with graphite carbon nitride, it is believed that these materials can mix together and as a result photocatalytic efficiency will increase substantially.[194, 196] For instance, g-C_3N_4 nanosheet was mixed with graphene in order to increase visible light photocatalytic activity for H_2 generation.[194] This metal-free nanocomposite could generate hydrogen from an aqueous solution of methanol under light illumination ($\lambda > 400$ nm). By using 1 wt% of graphene with Pt-loaded g-C_3N_4, the H_2 evolution rate noticeably enhanced from 147 μmol h^{-1} g^{-1} to 451 μmol h^{-1} g^{-1}. Another group tried

to modify g-C_3N_4 by introducing carbon nanotubes into its structure.[196] Despite the fact that the new composite and pure g-C_3N_4 are very similar in their properties, the new photocatalyst possessed higher activity (around 2.5 times) than the other one. With optimal amount of carbon nanotubes (2 wt%), it produced 394 μmol h^{-1} g^{-1} hydrogen under visible light illumination because of increasing the lifetime of excited electron and holes and prevent them to recombine together.

Furthermore, other semiconductors can be combined with g-C_3N_4 in order to prevent charge recombination. [192, 193, 197-202] For example, Chai et al. generated a nanocomposite consisting of porous g-C_3N_4 with TiO_2 nanoparticles.[192] According to the close interaction between these nanomaterials, when this nanocomposite improved by Pt metal as a cocatalyst, it showed hydrogen evolution under visible light illumination (λ > 420 nm). The maximum hydrogen evolution (178 μmol h^{-1}) was achieved when the mass ratio of g-C_3N_4 and TiO_2 was 70 to 30. Kang et al. synthesized a composite of graphitic carbon nitride and Rh-doped $SrTiO_3$.[193] By help of Pt as a cocatalyst, this photocatalyst could produce hydrogen from aqueous solution of methanol at 410 nm with a quantum yield of 5.5%. Doping Rh into the structure of $SrTiO_3$ provides the donor level in band gap region of $SrTiO_3$:Rh. As a result, the excited holes can easily transfer from $SrTiO_3$:Rh semiconductor to carbon nitride and the excited electrons move from the conduction band of g-C_3N_4 to $SrTiO_3$:Rh. This leads to have high charge separation and higher hydrogen production (2223 μmol h^{-1} g^{-1}) in comparison with each of the semiconductors alone.

Table 4: Different nanocomposite of graphitic carbon nitride

Semiconductor 1	Semiconductor 2	Cocatalyst	Sacrificial reagent	Light source	Hydrogen production (μmol h^{-1} g^{-1})	Quantum yield (%)	Refs
layered g-C_3N_4 sheets	graphitized polyacrylonitrile	Pt	Triethanolamine	150 W Halogen, λ ≥ 420 nm	370	No data	203
g-C_3N_4	Nickel sulfide (NiS)	---	Triethanolamine	300 W Xe, λ ≥ 420 nm	447.7	No data	197
g-C_3N_4	zinc phthalocyanine	Pt	Ascorbic acid	350 W Xe, λ ≥ 420 nm	12500	1.85 at λ = 700 nm	204
g-C_3N_4	C/N co-doped TiO2	Ag	Methanol	300 W Xe, λ ≥ 420 nm	96	No data	198
g-C_3N_4	PEDOT	Pt	Triethanolamine	300 W Xe, λ ≥ 420 nm	327	No data	195
g-C_3N_4	WO_3	Pt	Triethanolamine	300 W Xe, λ ≥ 420 nm	110	0.9 at λ = 420 nm	199
g-C_3N_4	carbon nanotubes	Pt	Triethanolamine	350 W Xe, λ ≥ 420 nm	394	No data	196
g-C_3N_4	$ZnFe_2O_4$	Pt	Triethanolamine	300 W Xe, λ ≥ 420 nm	200.77	No data	200
g-C_3N_4	Ag_2S	---	Methanol	300 W Xe, λ ≥ 420 nm	200	No data	201
g-C_3N_4	TiO_2	Pt	Triethanolamine	300 W Xe, λ ≥ 420 nm	1780	No data	192
g-C_3N_4	Poly(3-hexylthiophene)	Pt	Na_2S/Na_2SO_3	300 W Hg, λ ≥ 420 nm	1866	2.9 at λ = 420 nm	205
g-C_3N_4	Au nanoparticles	---	Triethanolamine	300 W Xe, λ ≥ 420 nm	8870	No data	206
C_3N_4	NiS	---	Triethanolamine	300 W Xe, λ ≥ 420 nm	482	1.99 at λ = 440 nm	207
Carbon nitride	N-doped tantalic acid	---	Methanol	300 W Xe, λ ≥ 420 nm	70.6	4.89 at λ = 420 nm	208
g-C_3N_4	$SrTiO_3$:Rh	Pt	Methanol	300 W Xe, λ ≥ 420 nm	2223	5.59 at λ = 420 nm	193
g-C_3N_4	MWNTs	Pt	Methanol	350 W Xe, λ ≥ 420 nm	75.8	No data	202

3.7. Other nanocomposites

In spite of above nanocomposites and nanostructures, scientists have tried to synthesize and combined other nanoscale semiconductors in order to achieve high efficient photocatalysts for hydrogen evolution under visible light illumination. 1D and 2D nanoparticles and nanostructures such as nanowires, nanotubes, nanorods, nanobelts, nanosheets, and nanoflates, have been interested among researchers in the last decade for water splitting via sunlight.[209-222] The combination of these kinds of nanostructures can enhance charge separation effectively and prevent the recombination process and so increase photocatalyst efficiency as summarized in Table 5.

Andrew Frame et al. found that CdSe nanoribbons were active in photocatalytic H_2 evolution from S^{2-}/SO_3^{2-} solution under visible light, whereas bulk CdSe was not.[217] By linking these nanoparticles with MoS_2 nanoplates, they activity enhanced about four times and so their quantum yields reached to 9.2% at 440 nm. Interestingly, in this nanocomposite Pt cannot be used as a cocatalyst due to sulfide poisoning of surface sites.

Jing et al. synthesized Cu-doped core/shell tubular nanocomposite of ZnO/ZnS.[218] They tried to deposit Cu-doped ZnS nanoparticles on the outside of ZnO nanotubes. As a result, this nanocomposite showed higher hydrogen evolution than undoped ZnO/ZnS nanocomposite. Copper ions act as donor level to induce visible light response of ZnS and thus excited electrons can migrate from ZnS to ZnO and from there they reduce protons.

Two ferrites chemical of calcium (CFO) and magnesium (MFO), i.e. $CaFe_2O_4$ and $MgFe_2O_4$ were used to synthesize nanocomposites for H_2 evolution reaction.[220] Due to the difference band position of these semiconductors, photoexcited electrons transfer from $CaFe_2O_4$ to $MgFe_2O_4$, whereas the holes can move vice versa. Both of CFO and MFO are active for hydrogen production under visible light irradiation when promoting with cocatalysts (Pt and RuO_2 for CFO and MFO, respectively). However, the nanocomposite of CFO and MFO produced 82.8 mmol h^{-1} g^{-1} with quantum yield of 10.1% which was an order of magnitude higher than RuO_2/MFO or Pt/CFO.

Pradhan et al. synthesized mesoporous nanocomposite of Fe/Al_2O_3–MCM-41 with size of 50 nm. They reported that this photocatalysts with 5 wt% of Fe had the hydrogen production activity under visible light (146 μmol h^{-1}) with the quantum yield of 6.1%. The main reason for such activity is due to the

properties of mesoporous materials which are high pore volume, narrow pore size distribution and high surface area. Furthermore, iron doping on the surface helped to absorb visible light, although the mesoporous nanocomposite by itself didn't show any activity for λ > 400 nm.[221]

Table 5: Other nanocomposites for hydrogen production under visible light irradiation.

Semiconductor 1	Semiconductor 2	Cocatalyst	Sacrificial reagent	Light source	Hydrogen production (μmol h^{-1} g^{-1})	Quantum yield (%)	Refs
ZnS	ZnO core/shell nanotube	Pt	Na_2S/Na_2SO_3	300 W Xe, λ ≥ 420 nm	18	No data	218
$NaNbO_3$ nanorods	In_2O_3 nanoparticles	Pt	Methanol	300 W Xe, λ ≥ 420 nm	16.4	1.45 at λ = 420 nm	219
$MgFe_2O_4$	$CaFe_2O_4$	RuO2 on guest and Pt on host	Methanol	450 W W-Arc, λ ≥ 420 nm	82.1	10.1 at λ = 420 nm	220
Al_2O_3–MCM-41	Fe	---	Methanol	150 W Hg, λ ≥ 400 nm	1460	6.1 at λ = 400 nm	221
Fe_2O_3	Fe_4N	---	---	300 W Xe, λ ≥ 420 nm	25	1.7 at λ = 400 nm	222
WO_3	Au	Pt	Glycerol	300 W Xe, λ ≥ 420 nm	132	0.2 at λ = 420 nm	223
Ta_2O_5 Ta_3N_5	Au	Pt	Methanol	350 W Xe, λ ≥ 420 nm	55 150	No data	224
ZnS–Bi_2S_3 nanorods	ZnO	---	Glycerol	300 W Xe, λ ≥ 420 nm	310	No data	225
Rh-doped $SrTiO_3$	$BiVO_4$	Ru	---	350 W Xe, λ ≥ 420 nm	200	1.6 at λ = 400 nm	226
ZnO	In_2O_3	---	Methanol	300 W Xe, λ ≥ 420 nm	1784	No data	227
$SrTiO_3$ (La,Cr)	Sr_2TiO_4	Pt	Methanol	300 W Xe, λ ≥ 420 nm	24	No data	228
Bi–$NaTaO_3$	Bi_2O_3	---	Methanol	300 W Xe, λ ≥ 420 nm	102.5	No data	229
$GdCrO_3$	$Gd_2Ti_2O_7$	---	Methanol	350 W Hg, λ ≥ 400 nm	1231.5	4.1 at λ = 400 nm	230
$Ag_3PW_{12}O_{40}$	Carbon quantum dots	Ag	---	300 W Xe, λ ≥ 420 nm	3.8	4.9 at λ = 480 nm	231
$Cu_{1.8}S$	ZnS	---	Na_2S/Na_2SO_3	300 W Xe, λ ≥ 420 nm	467	No data	232
2D ultrathin curled $ZnIn_2S_4$ nanosheet	MoS_2	---	Na_2S/Na_2SO_3	300 W Xe, λ ≥ 420 nm	975	No data	233
In_2O_3	$Gd_2Ti_2O_7$	---	Methanol	300 W Xe, λ ≥ 420 nm	5789	No data	234
$K_2La_2Ti_3O_{10}$	$ZnIn_2S_4$	---	Na_2S/Na_2SO_3	300 W Xe, λ ≥ 420 nm	2096	No data	235
Ta_2O_5	In_2O_3	Pt	Methanol	300 W Xe, λ ≥ 420 nm	10	No data	236

4. Conclusion

Photocatalytic hydrogen production based on solar-driven water splitting is one of the best ways to use solar energy. However, industrial application of this strategy is still hindered by its currently low efficiency originated from the lack of efficient photocatalysts. Various methods have been developed to boost the photocatalyst efficiency such as metal or non-metal doping of wide band-gap semiconductors to decrease their band gap and applying cocatalysts to improve the charge separation and to provide active sites on the surface of semiconductor for water splitting. Making multicomponent heterojunctions of different semiconductor nanocomposites offer an effective tool to extent sunlight absorption and also to increase charge carrier lifetimes by enhancing charge separation. Nanostructured photocatalysts can improve the efficiency by providing large surface area and small particle size. As a result, charge carriers transfer noticeably small distances from the bulk material to its surface that partially limited a recombination phenomenon.

Among various semiconductor heterojunction for photocatalytic hydrogen generation, TiO_2 and CdS based systems have been most studied. TiO_2 is one of the applicable and commercial photocatalysts that can be utilized in different photocatalysis processes. Combining nano-sized TiO_2 with suitable small band-gap semiconductors produces nanocomposite photocatalysts which exhibit an improvement for hydrogen production in the visible light region. CdS, on the other hand, has been widely studied for hydrogen production because of its relatively small band-gap and suitable electronic band structure. Combining CdS with other semiconductors helps to improve the charge separation and stability of CdS which lead to the formation of efficient nanocomposites for hydrogen generation. Currently, CdS based photocatalysts are among the best photocatalysts for hydrogen generation under the visible light.

Although coupling semiconductors has been shown to improve the photocatalytic efficiency of the photocatalyst, the overall efficiency for hydrogen production using sunlight is still very low. Factors such as composition, interface between the semiconductors, and morphology of each component, all of which determine the photocatalytic activity of such materials, need to be further elucidated in great detail. Furthermore, the charge transfer in multi-component photocatalysts is sensitively and greatly affected by how the hybrid is organized. Thus, the relative position of each semiconductor and cocatalysts need to be controlled in order to optimize the electron transfer throughout the photocatalyst. Besides, new material design and innovative strategies for improving charge separation and sunlight absorption of the photocatalysts are also very important for the realization of hydrogen production based on solar driven water splitting.

Biographical Information

Mohamad Reza Gholipour obtained his BSc and MSc degrees in Chemical Engineering from Shiraz University, in 2009 and 2012, respectively. He is currently working for his PhD degree at Laval University, Canada under the supervision of Prof. Trong-On Do. He focuses on the synthesis and development of nanocomposite photocatalysts for water splitting via solar energy.

Cao-Thang Dinh studied chemical engineering at Laval University under the guidance of Prof. Trong-On Do where he received his Master in 2011 and PhD in 2014. After graduation, he joined Prof. Edward Sargent's group at the University of Toronto as a Postdoctoral Fellow. He received his BSc at Hanoi University of Mining and Geology in 2004. He worked at Vietnam Academy of Science and Technology from 2005 to 2008. Cao-Thang's current research focuses on the synthesis of multi-functional photocatalysts for the production of solar fuels from water and carbon dioxide.

Francois Béland is currently the Vice President of R&D at SiliCycle. He earned his Ph.D. in 1999 from Laval University in Quebec City where he studied silica based catalysts by different spectroscopy methods. Francois then traveled to the South of France for his post-doctoral studies at the Ecole Nationale Supérieure de Chimie de Montpellier. There he studied different catalytic reactions in organic chemistry catalyzed by silica-based heterogeneous catalysts. After his post-doc work, he started his career at SiliCycle as a researcher. After his promotion to R&D Director, his focus was to develop the SiliaBond (functionalized silica gels) product line. Dr. Béland has 15 years of experience with silica-based products for different applications in chromatography and organic chemistry.

Trong-On Do is a full professor in the Department of Chemical Engineering at Laval University, Canada. He received his MSc in 1986 and PhD in 1989 at University of P. and M. Curie (Paris 6, France). After a period at Brunel University (UK) and the French Catalysis Institute (France), he moved to Laval University in 1990. He then spent two years 1997-1999 in Profs. Hashimoto/Fujishima's group at Kanagawa Academy of Science and Technology under the Japanese STA Fellowship Award before re-joining Laval University as a professor associated with the NSERC Industrial chair. He has published over 120 papers and review articles in refereed journals and holds 5 international patents. He is the recipient of the 2014 Canadian Catalysis Lectureship Award (CCLA).

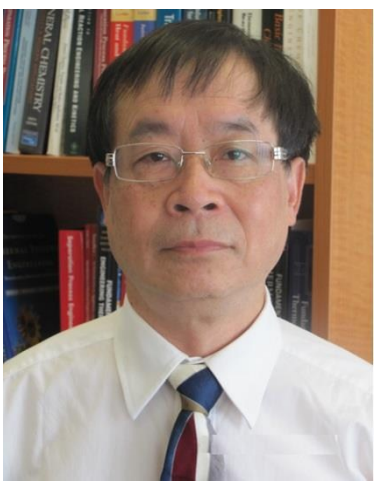

5. Notes and references

[a] Department of Chemical Engineering, Université Laval, Québec, G1V 0A6, Canada; [b] SiliCycle Inc., 2500, Boul. du Parc-Technologique Québec (QC) G1P 4S6, Canada.

1. N. S. Lewis and D. G. Nocera, *Proceedings of the National Academy of Sciences*, 2006, 103, 15729-15735.
2. W. Fan, Q. Zhang and Y. Wang, *Physical Chemistry Chemical Physics*, 2013, 15, 2632-2649.

3. A. Fujishima, *nature*, 1972, 238, 37-38.
4. A. J. Bard, *Journal of Photochemistry*, 1979, 10, 59-75.
5. B. D. Alexander, P. J. Kulesza, I. Rutkowska, R. Solarska and J. Augustynski, *Journal of Materials Chemistry*, 2008, 18, 2298-2303.
6. T. Bak, J. Nowotny, M. Rekas and C. Sorrell, *International journal of hydrogen energy*, 2002, 27, 991-1022.
7. A. Kudo and Y. Miseki, *Chemical Society Reviews*, 2009, 38, 253-278.
8. D. Zhang, G. Li, H. Li and Y. Lu, *Chemistry–An Asian Journal*, 2013, 8, 26-40.
9. Y. Sang, H. Liu and A. Umar, *ChemCatChem*, 2014, DOI: 10.1002/cctc.201402812, n/a-n/a.
10. Y. Tang, W. Di, X. Zhai, R. Yang and W. Qin, *ACS Catalysis*, 2013, 3, 405-412.
11. S. Shen, J. Shi, P. Guo and L. Guo, *International Journal of Nanotechnology*, 2011, 8, 523-591.
12. J. Nowotny, C. Sorrell, T. Bak and L. Sheppard, *Solar Energy*, 2005, 78, 593-602.
13. Z. Zou, J. Ye, K. Sayama and H. Arakawa, *Nature*, 2001, 414, 625-627.
14. X. Chen, S. Shen, L. Guo and S. S. Mao, *Chemical Reviews*, 2010, 110, 6503-6570.
15. K. Maeda, K. Teramura and K. Domen, *Journal of catalysis*, 2008, 254, 198-204.
16. A. J. Esswein and D. G. Nocera, *Chemical Reviews*, 2007, 107, 4022-4047.
17. A. Galińska and J. Walendziewski, *Energy & Fuels*, 2005, 19, 1143-1147.
18. J. Wang, P. Yang, B. Cao, J. Zhao and Z. Zhu, *Applied Surface Science*, 2015, 325, 86-90.
19. F. Guzman, S. S. C. Chuang and C. Yang, *Industrial & Engineering Chemistry Research*, 2012, 52, 61-65.
20. T. Kawai and T. Sakata, *Journal of the Chemical Society, Chemical Communications*, 1979, 1047-1048.
21. T. Kawai and T. Sakata, *Journal of the Chemical Society, Chemical Communications*, 1980, 694-695.
22. P. Zhou, J. Yu and M. Jaroniec, *Advanced Materials*, 2014, DOI: 10.1002/adma.201400288, n/a-n/a.
23. X. Zong, G. Lu and L. Wang, *Nanocatalysis Synthesis and Applications*, 2013, 495-559.
24. P. Zhou, J. Yu and M. Jaroniec, *Advanced Materials*, 2014, 26, 4920-4935.
25. K. Maeda, *ACS Catalysis*, 2013, 3, 1486-1503.
26. K. Sayama, K. Mukasa, R. Abe, Y. Abe and H. Arakawa, *Journal of Photochemistry and Photobiology A: Chemistry*, 2002, 148, 71-77.
27. N. Serpone, G. Sauve, R. Koch, H. Tahiri, P. Pichat, P. Piccinini, E. Pelizzetti and H. Hidaka, *Journal of photochemistry and photobiology A: Chemistry*, 1996, 94, 191-203.
28. S. Khan and S. Majumder, *International journal of hydrogen energy*, 1989, 14, 653-660.
29. J. Akikusa and S. U. Khan, *International journal of hydrogen energy*, 2002, 27, 863-870.
30. K. Gurunathan, *International Journal of Hydrogen Energy*, 2004, 29, 933-940.
31. J. S. Jang, K. Y. Yoon, X. Xiao, F.-R. F. Fan and A. J. Bard, *Chemistry of Materials*, 2009, 21, 4803-4810.
32. J. S. Jang, S. H. Choi, H. G. Kim and J. S. Lee, *The Journal of Physical Chemistry C*, 2008, 112, 17200-17205.
33. K. Maeda, K. Teramura, D. Lu, N. Saito, Y. Inoue and K. Domen, *Angewandte Chemie*, 2006, 118, 7970-7973.
34. K. Domen, S. Naito, T. Onishi and K. Tamaru, *Chemical Physics Letters*, 1982, 92, 433-434.
35. S. Sato and J. White, *Chemical Physics Letters*, 1980, 72, 83-86.
36. J. Lehn, J. Sauvage, R. Zlessel and L. Hilaire, *Israel Journal of Chemistry*, 1982, 22, 168-172.
37. K. Yamaguti and S. Sato, *Journal of the Chemical Society, Faraday Transactions 1: Physical Chemistry in Condensed Phases*, 1985, 81, 1237-1246.
38. A. Iwase, H. Kato and A. Kudo, *Catalysis letters*, 2006, 108, 7-10.
39. Y. Inoue, O. Hayashi and K. Sato, *J. Chem. Soc., Faraday Trans.*, 1990, 86, 2277-2282.
40. K. Maeda, K. Teramura, N. Saito, Y. Inoue and K. Domen, *Journal of Catalysis*, 2006, 243, 303-308.
41. H. Sheng, L. Yu, Y. Jian-Hua and Y. Ying, in *Nanotechnology for Sustainable Energy*, American Chemical Society, 2013, vol. 1140, ch. 9, pp. 219-241.
42. R. Marschall, *Advanced Functional Materials*, 2014, 24, 2421-2440.
43. A. L. Linsebigler, G. Lu and J. T. Yates Jr, *Chemical reviews*, 1995, 95, 735-758.
44. M. Sathish, B. Viswanathan and R. Viswanath, *International Journal of Hydrogen Energy*, 2006, 31, 891-898.
45. P. S. Lunawat, R. Kumar and N. M. Gupta, *Catalysis Letters*, 2008, 121, 226-233.
46. K. Parida, K. Reddy, S. Martha, D. Das and N. Biswal, *International journal of hydrogen energy*, 2010, 35, 12161-12168.
47. L. Yuliati, J.-H. Yang, X. Wang, K. Maeda, T. Takata, M. Antonietti and K. Domen, *Journal of Materials Chemistry*, 2010, 20, 4295-4298.
48. Z. Zhang, C.-C. Wang, R. Zakaria and J. Y. Ying, *The Journal of Physical Chemistry B*, 1998, 102, 10871-10878.
49. N. Serpone, D. Lawless, R. Khairutdinov and E. Pelizzetti, *The Journal of Physical Chemistry*, 1995, 99, 16655-16661.
50. T. Ishihara, N. S. Baik, N. Ono, H. Nishiguchi and Y. Takita, *Journal of Photochemistry and Photobiology A: Chemistry*, 2004, 167, 149-157.
51. N. Bao, L. Shen, T. Takata, K. Domen, A. Gupta, K. Yanagisawa and C. A. Grimes, *The Journal of Physical Chemistry C*, 2007, 111, 17527-17534.
52. I. Gur, N. A. Fromer, M. L. Geier and A. P. Alivisatos, *Science*, 2005, 310, 462-465.
53. J. S. Steckel, J. P. Zimmer, S. Coe-Sullivan, N. E. Stott, V. Bulović and M. G. Bawendi, *Angewandte Chemie International Edition*, 2004, 43, 2154-2158.
54. Y. Ohko, T. Tatsuma, T. Fujii, K. Naoi, C. Niwa, Y. Kubota and A. Fujishima, *Nature Materials*, 2003, 2, 29-31.
55. X. Wang, G. Liu, L. Wang, Z. G. Chen, G. Q. M. Lu and H. M. Cheng, *Advanced Energy Materials*, 2012, 2, 42-46.
56. J. Zhu and M. Zäch, *Current Opinion in Colloid & Interface Science*, 2009, 14, 260-269.
57. S.-D. Mo and W. Ching, *Physical Review B*, 1995, 51, 13023.
58. Y. Liu, L. Guo, W. Yan and H. Liu, *Journal of Power Sources*, 2006, 159, 1300-1304.
59. H. Yang, L. Guo, W. Yan and H. Liu, *Journal of Power Sources*, 2006, 159, 1305-1309.
60. B. Naik, S. Martha and K. Parida, *International journal of hydrogen energy*, 2011, 36, 2794-2802.
61. S. Martha, D. P. Das, N. Biswal and K. M. Parida, *Journal of Materials Chemistry*, 2012, 22, 10695-10703.
62. M. Xie, X. Fu, L. Jing, P. Luan, Y. Feng and H. Fu, *Advanced Energy Materials*, 2014, 4, n/a-n/a.
63. W. Yan, Y. Zhang, W. Xie, S. Sun, J. Ding, J. Bao and C. Gao, *The Journal of Physical Chemistry C*, 2014, 118, 6077-6083.
64. S. Zhu, F. Yao, C. Yin, Y. Li, W. Peng, J. Ma and D. Zhang, *Microporous and Mesoporous Materials*, 2014, 190, 10-16.
65. M. Xie, X. Fu, L. Jing, P. Luan, Y. Feng and H. Fu, *Advanced Energy Materials*, 2013.
66. Y. H. Ng, A. Iwase, A. Kudo and R. Amal, *J. Phys. Chem. Lett*, 2010, 1, 2607-2612.
67. K. E. deKrafft, C. Wang and W. Lin, *Advanced Materials*, 2012, 24, 2014-2018.
68. E. Thimsen, S. Biswas, C. S. Lo and P. Biswas, *The Journal of Physical Chemistry C*, 2009, 113, 2014-2021.
69. M.-H. Pham, T. C. Dinh, G.-T. Vuong, N.-D. Ta and T.-O. Do, *Physical Chemistry Chemical Physics*, 2014.
70. S. K. Sarkar, J. Y. Kim, D. N. Goldstein, N. R. Neale, K. Zhu, C. M. Elliott, A. J. Frank and S. M. George, *The Journal of Physical Chemistry C*, 2010, 114, 8032-8039.
71. B. Chai, T. Peng, P. Zeng and J. Mao, *Journal of Materials Chemistry*, 2011, 21, 14587-14593.
72. S. Shen and L. Guo, *Journal of Solid State Chemistry*, 2006, 179, 2629-2635.
73. K. Li, B. Chai, T. Peng, J. Mao and L. Zan, *ACS Catalysis*, 2013, 3, 170-177.

74. J. S. Jang, S. J. Hong, J. Y. Kim and J. S. Lee, *Chemical Physics Letters*, 2009, 475, 78-81.
75. P. Zeng, X. Zhang, X. Zhang, B. Chai and T. Peng, *Chemical Physics Letters*, 2011, 503, 262-265.
76. H. Yu, Y. Zhao, C. Zhou, L. Shang, Y. Peng, Y. Cao, L.-Z. Wu, C.-H. Tung and T. Zhang, *Journal of Materials Chemistry A*, 2013.
77. H. Yu, Y. Zhao, C. Zhou, L. Shang, Y. Peng, Y. Cao, L.-Z. Wu, C.-H. Tung and T. Zhang, *Journal of Materials Chemistry A*, 2014, 2, 3344-3351.
78. Y. Ou, J. Lin, S. Fang and D. Liao, *Chemical Physics Letters*, 2006, 429, 199-203.
79. Q. Xiang, J. Yu and M. Jaroniec, *Nanoscale*, 2011, 3, 3670-3678.
80. Y. Wang, J. Yu, W. Xiao and Q. Li, *Journal of Materials Chemistry A*, 2014, 2, 3847-3855.
81. P. Brown and P. V. Kamat, *Journal of the American Chemical Society*, 2008, 130, 8890-8891.
82. X.-Y. Zhang, H.-P. Li, X.-L. Cui and Y. Lin, *Journal of Materials Chemistry*, 2010, 20, 2801-2806.
83. Z. Bian, T. Tachikawa, P. Zhang, M. Fujitsuka and T. Majima, *Journal of the American Chemical Society*, 2013, 136, 458-465.
84. M.-H. Pham, C.-T. Dinh, G.-T. Vuong, N.-D. Ta and T.-O. Do, *Physical Chemistry Chemical Physics*, 2014, 16, 5937-5941.
85. D. Jing and L. Guo, *Catalysis Communications*, 2007, 8, 795-799.
86. D. Jing and L. Guo, *The Journal of Physical Chemistry B*, 2006, 110, 11139-11145.
87. N. Bao, L. Shen, T. Takata and K. Domen, *Chemistry of Materials*, 2007, 20, 110-117.
88. J. Cao, J. Z. Sun, J. Hong, H. Y. Li, H. Z. Chen and M. Wang, *Advanced Materials*, 2004, 16, 84-87.
89. X. Wang, G. Liu, G. Q. Lu and H.-M. Cheng, *international journal of hydrogen energy*, 2010, 35, 8199-8205.
90. G. QingáLu, *Chemical Communications*, 2009, 3452-3454.
91. J. Hou, Z. Wang, W. Kan, S. Jiao, H. Zhu and R. Kumar, *Journal of Materials Chemistry*, 2012, 22, 7291-7299.
92. X. Zou, P.-P. Wang, C. Li, J. Zhao, D. Wang, T. Asefa and G.-D. Li, *Journal of Materials Chemistry A*, 2014.
93. X.-H. Lu, S.-L. Xie, T. Zhai, Y.-F. Zhao, P. Zhang, Y.-L. Zhang and Y.-X. Tong, *RSC Advances*, 2011, 1, 1207-1210.
94. X. Zou, P.-P. Wang, C. Li, J. Zhao, D. Wang, T. Asefa and G.-D. Li, *Journal of Materials Chemistry A*, 2014, 2, 4682-4689.
95. X. Cui, Y. Wang, G. Jiang, Z. Zhao, C. Xu, Y. Wei, A. Duan, J. Liu and J. Gao, *RSC Advances*, 2014, 4, 15689-15694.
96. Z. Wang, J. Hou, C. Yang, S. Jiao and H. Zhu, *Chemical Communications*, 2014, 50, 1731-1734.
97. G. Yang, W. Yan, Q. Zhang, S. Shen and S. Ding, *Nanoscale*, 2013, 5, 12432-12439.
98. Z. Shen, G. Chen, Y. Yu, Q. Wang, C. Zhou, L. Hao, Y. Li, L. He and R. Mu, *Journal of Materials Chemistry*, 2012, 22, 19646-19651.
99. Y.-x. Pan, H. Zhuang, J. Hong, Z. Fang, H. Liu, B. Liu, Y. Huang and R. Xu, *ChemSusChem*, 2014, 7, 2537-2544.
100. L. Wang and W. Wang, *CrystEngComm*, 2012, 14, 3315-3320.
101. T. Kida, G. Guan and A. Yoshida, *Chemical physics letters*, 2003, 371, 563-567.
102. J. Choi, S. Y. Ryu, W. Balcerski, T. Lee and M. R. Hoffmann, *Journal of Materials Chemistry*, 2008, 18, 2371-2378.
103. S. Y. Ryu, J. Choi, W. Balcerski, T. K. Lee and M. R. Hoffmann, *Industrial & Engineering Chemistry Research*, 2007, 46, 7476-7488.
104. Z. Shen, G. Chen, Q. Wang, Y. Yu, C. Zhou and Y. Wang, *Nanoscale*, 2012, 4, 2010-2017.
105. Z. Khan, T. R. Chetia and M. Qureshi, *Nanoscale*, 2012, 4, 3543-3550.
106. U. Gupta, B. G. Rao, U. Maitra, B. E. Prasad and C. N. R. Rao, *Chemistry – An Asian Journal*, 2014, 9, 1311-1315.
107. W. Zhang, Z. Zhong, Y. Wang and R. Xu, *The Journal of Physical Chemistry C*, 2008, 112, 17635-17642.
108. L. Ren, F. Yang, Y.-R. Deng, N.-N. Yan, S. Huang, D. Lei, Q. Sun and Y. Yu, *International journal of hydrogen energy*, 2010, 35, 3297-3305.
109. W. Zhang, Z. Zhong, Y. Wang and R. Xu, *Journal of Physical Chemistry C*, 2008, 112, 17635-17642.
110. M. Liu, L. Wang, G. M. Lu, X. Yao and L. Guo, *Energy & Environmental Science*, 2011, 4, 1372-1378.
111. J. F. Reber and M. Rusek, *The Journal of Physical Chemistry*, 1986, 90, 824-834.
112. A. Deshpande, P. Shah, R. Gholap and N. M. Gupta, *Journal of colloid and interface science*, 2009, 333, 263-268.
113. S. R. Lingampalli, U. K. Gautam and C. N. R. Rao, *Energy & Environmental Science*, 2013, 6, 3589-3594.
114. J. Hou, C. Yang, Z. Wang, S. Jiao and H. Zhu, *RSC Advances*, 2012, 2, 10330-10336.
115. X. Zong, H. Yan, G. Wu, G. Ma, F. Wen, L. Wang and C. Li, *Journal of the American Chemical Society*, 2008, 130, 7176-7177.
116. J. S. Jang, D. J. Ham, N. Lakshminarasimhan and J. S. Lee, *Applied Catalysis A: General*, 2008, 346, 149-154.
117. W. Zhang, Y. Wang, Z. Wang, Z. Zhong and R. Xu, *Chemical Communications*, 2010, 46, 7631-7633.
118. H. Yan, J. Yang, G. Ma, G. Wu, X. Zong, Z. Lei, J. Shi and C. Li, *Journal of Catalysis*, 2009, 266, 165-168.
119. L. Yuliati, M. Kimi and M. Shamsuddin, *Beilstein Journal of Nanotechnology*, 2014, 5, 587-595.
120. T. Peng, P. Zeng, D. Ke, X. Liu and X. Zhang, *Energy & Fuels*, 2011, 25, 2203-2210.
121. Y. K. Kim and H. Park, *Energy & Environmental Science*, 2011, 4, 685-694.
122. J. Yu, B. Yang and B. Cheng, *Nanoscale*, 2012, 4, 2670-2677.
123. L. Wang, Z. Yao, F. Jia, B. Chen and Z. Jiang, *Dalton Transactions*, 2013, 42, 9976-9981.
124. X. Wang, M. Liu, Q. Chen, K. Zhang, J. Chen, M. Wang, P. Guo and L. Guo, *International Journal of Hydrogen Energy*, 2013, 38, 13091-13096.
125. A. Ye, W. Fan, Q. Zhang, W. Deng and Y. Wang, *Catalysis Science & Technology*, 2012, 2, 969-978.
126. K. S. Novoselov, *Angewandte Chemie International Edition*, 2011, 50, 6986-7002.
127. X.-J. Lv, W.-F. Fu, H.-X. Chang, H. Zhang, J.-S. Cheng, G.-J. Zhang, Y. Song, C.-Y. Hu and J.-H. Li, *Journal of Materials Chemistry*, 2012, 22, 1539-1546.
128. J. Wang, P. Yang, J. Zhao and Z. Zhu, *Applied Surface Science*, 2013, 282, 930-936.
129. Q. Li, H. Meng, J. Yu, W. Xiao, Y. Zheng and J. Wang, *Chemistry-A European Journal*, 2014, 20, 1176-1185.
130. L. Jia, D.-H. Wang, Y.-X. Huang, A.-W. Xu and H.-Q. Yu, *The Journal of Physical Chemistry C*, 2011, 115, 11466-11473.
131. K. Chang, Z. Mei, T. Wang, Q. Kang, S. Ouyang and J. Ye, *ACS Nano*, 2014, 8, 7078-7087.
132. J. Hou, C. Yang, H. Cheng, Z. Wang, S. Jiao and H. Zhu, *Physical Chemistry Chemical Physics*, 2013, 15, 15660-15668.
133. Q. Li, B. Guo, J. Yu, J. Ran, B. Zhang, H. Yan and J. R. Gong, *Journal of the American Chemical Society*, 2011, 133, 10878-10884.
134. J. Liu, H. Bai, Y. Wang, Z. Liu, X. Zhang and D. D. Sun, *Advanced Functional Materials*, 2010, 20, 4175-4181.
135. T.-D. Nguyen-Phan, V. H. Pham, E. W. Shin, H.-D. Pham, S. Kim, J. S. Chung, E. J. Kim and S. H. Hur, *Chemical Engineering Journal*, 2011, 170, 226-232.
136. Q. Xiang, J. Yu and M. Jaroniec, *Chemical Society Reviews*, 2012, 41, 782-796.
137. T. Peng, K. Li, P. Zeng, Q. Zhang and X. Zhang, *The Journal of Physical Chemistry C*, 2012, 116, 22720-22726.
138. Z. Yan, X. Yu, A. Han, P. Xu and P. Du, *The Journal of Physical Chemistry C*, 2014, DOI: 10.1021/jp5065402.
139. P. Zeng, Q. Zhang, T. Peng and X. Zhang, *Physical Chemistry Chemical Physics*, 2011, 13, 21496-21502.
140. X. Tang, Q. Tay, Z. Chen, Y. Chen, G. K. L. Goh and J. Xue, *Journal of Materials Chemistry A*, 2013, 1, 6359-6365.
141. R. Lin, L. Shen, Z. Ren, W. Wu, Y. Tan, H. Fu, J. Zhang and L. Wu, *Chemical Communications*, 2014, 50, 8533-8535.
142. Y. Li, H. Wang and S. Peng, *The Journal of Physical Chemistry C*, 2014, 118, 19842-19848.
143. J. Zhang, J. Yu, M. Jaroniec and J. R. Gong, *Nano letters*, 2012, 12, 4584-4589.

144. F. Schedin, A. Geim, S. Morozov, E. Hill, P. Blake, M. Katsnelson and K. Novoselov, *Nature materials*, 2007, 6, 652-655.
145. X. Wang, L. Yin and G. Liu, *Chemical Communications*, 2014, 50, 3460-3463.
146. P. Zeng, Q. Zhang, T. Peng and X. Zhang, *Physical Chemistry Chemical Physics*, 2011, 13, 21496-21502.
147. W. Tu, Y. Zhou and Z. Zou, *Advanced Functional Materials*, 2013, 23, 4996-5008.
148. S. Bai and X. Shen, *Rsc Advances*, 2012, 2, 64-98.
149. L. Amirav and A. P. Alivisatos, *The Journal of Physical Chemistry Letters*, 2010, 1, 1051-1054.
150. T. Kida, G. Guan, Y. Minami, T. Ma and A. Yoshida, *Journal of Materials Chemistry*, 2003, 13, 1186-1191.
151. J. Zhang, S. Z. Qiao, L. Qi and J. Yu, *Physical Chemistry Chemical Physics*, 2013, 15, 12088-12094.
152. X. Wang, W.-c. Peng and X.-y. Li, *International Journal of Hydrogen Energy*, 2014, 39, 13454-13461.
153. J. Zhang, W. Zhu and X. Liu, *Dalton Transactions*, 2014, 43, 9296-9302.
154. Y. Peng, Z. Guo, J. Yang, D. Wang and W. Yuan, *Journal of Materials Chemistry A*, 2014, 2, 6296-6300.
155. M. Khatamian, M. Saket Oskoui and M. Haghighi, *New Journal of Chemistry*, 2014, 38, 1684-1693.
156. R. Peng, C.-M. Wu, J. Baltrusaitis, N. M. Dimitrijevic, T. Rajh and R. T. Koodali, *Chemical Communications*, 2013, 49, 3221-3223.
157. R. Peng, D. Zhao, J. Baltrusaitis, C.-M. Wu and R. T. Koodali, *RSC Advances*, 2012, 2, 5754-5767.
158. Z. Liu, S. Shen and L. Guo, *International Journal of Hydrogen Energy*, 2012, 37, 816-821.
159. J. S. Jang, D. W. Hwang and J. S. Lee, *Catalysis Today*, 2007, 120, 174-181.
160. L. Ge, F. Zuo, J. Liu, Q. Ma, C. Wang, D. Sun, L. Bartels and P. Feng, *The Journal of Physical Chemistry C*, 2012, 116, 13708-13714.
161. J. S. Jang, S. M. Ji, S. W. Bae, H. C. Son and J. S. Lee, *Journal of photochemistry and photobiology. A, Chemistry*, 2007, 188, 112-119.
162. J. S. Jang, H. G. Kim, U. A. Joshi, J. W. Jang and J. S. Lee, *International Journal of Hydrogen Energy*, 2008, 33, 5975-5980.
163. Y. Chen, L. Wang, G. M. Lu, X. Yao and L. Guo, *Journal of Materials Chemistry*, 2011, 21, 5134-5141.
164. C. Li, J. Yuan, B. Han, L. Jiang and W. Shangguan, *International journal of hydrogen energy*, 2010, 35, 7073-7079.
165. C. Xing, D. Jing, M. Liu and L. Guo, *Materials Research Bulletin*, 2009, 44, 442-445.
166. Y. J. Zhang, Y. C. Wang, W. Yan, T. Li, S. Li and Y. R. Hu, *Applied Surface Science*, 2009, 255, 9508-9511.
167. C. Xing, D. Jing, M. Liu and L. Guo, *Materials Research Bulletin*, 2009, 44, 442-445.
168. T. T. D. Vu, F. Mighri, A. Ajji and T.-O. Do, *Industrial & Engineering Chemistry Research*, 2014, 53, 3888-3897.
169. H. N. Kim, T. W. Kim, I. Y. Kim and S. J. Hwang, *Advanced Functional Materials*, 2011, 21, 3111-3118.
170. T. C. Dinh, M.-H. Pham, Y. Seo, F. Kleitz and T.-O. Do, *Nanoscale*, 2014.
171. D. He, M. Chen, F. Teng, G. Li, H. Shi, J. Wang, M. Xu, T. Lu, X. Ji and Y. Lv, *Superlattices and Microstructures*, 2012, 51, 799-808.
172. L. Qi, J. Yu and M. Jaroniec, *Physical Chemistry Chemical Physics*, 2011, 13, 8915-8923.
173. H. N. Kim, T. W. Kim, I. Y. Kim and S.-J. Hwang, *Advanced Functional Materials*, 2011, 21, 3111-3118.
174. D. He, M. Chen, F. Teng, G. Li, H. Shi, J. Wang, M. Xu, T. Lu, X. Ji, Y. Lv and Y. Zhu, *Superlattices and Microstructures*, 2012, 51, 799-808.
175. C.-T. Dinh, M.-H. Pham, F. Kleitz and T.-O. Do, *Journal of Materials Chemistry A*, 2013, 1, 13308-13313.
176. T. D. Nguyen, C. T. Dinh and T. O. Do, *Chem Commun (Camb)*, 2014, DOI: 10.1039/c4cc05741d.
177. H. Park, Y. K. Kim and W. Choi, *The Journal of Physical Chemistry C*, 2011, 115, 6141-6148.
178. M. Khatamian, M. Saket Oskoui, M. Haghighi and M. Darbandi, *International Journal of Energy Research*, 2014.
179. Y. Chen and L. Guo, *Journal of Materials Chemistry*, 2012, 22, 7507-7514.
180. H. Park, W. Choi and M. R. Hoffmann, *Journal of Materials Chemistry*, 2008, 18, 2379-2385.
181. Y. Zhang, Y. Tang, X. Liu, Z. Dong, H. H. Hng, Z. Chen, T. C. Sum and X. Chen, *Small*, 2013, 9, 996-1002.
182. M. de Oliveira Melo and L. A. Silva, *Journal of Photochemistry and Photobiology A: Chemistry*, 2011, 226, 36-41.
183. J. S. Jang, H. G. Kim, U. A. Joshi, J. W. Jang and J. S. Lee, *International Journal of Hydrogen Energy*, 2008, 33, 5975-5980.
184. J. S. Jang, W. Li, S. H. Oh and J. S. Lee, *Chemical Physics Letters*, 2006, 425, 278-282.
185. M. S. Oskoui, M. Khatamian, M. Haghighi and A. Yavari, *RSC Advances*, 2014, 4, 19569-19577.
186. J. Fang, L. Xu, Z. Zhang, Y. Yuan, S. Cao, Z. Wang, L. Yin, Y. Liao and C. Xue, *ACS applied materials & interfaces*, 2013, 5, 8088-8092.
187. X.-F. Wu, H.-Y. Song, J.-M. Yoon, Y.-T. Yu and Y.-F. Chen, *Langmuir*, 2009, 25, 6438-6447.
188. Y. Wang, X. Wang and M. Antonietti, *Angewandte Chemie International Edition*, 2012, 51, 68-89.
189. X. Wang, K. Maeda, A. Thomas, K. Takanabe, G. Xin, J. M. Carlsson, K. Domen and M. Antonietti, *Nat Mater*, 2009, 8, 76-80.
190. S. Cao and J. Yu, *The Journal of Physical Chemistry Letters*, 2014, 5, 2101-2107.
191. Z. Zhao, Y. Sun and F. Dong, *Nanoscale*, 2014, DOI: 10.1039/C4NR03008G.
192. B. Chai, T. Peng, J. Mao, K. Li and L. Zan, *Physical Chemistry Chemical Physics*, 2012, 14, 16745-16752.
193. H. W. Kang, S. N. Lim, D. Song and S. B. Park, *International Journal of Hydrogen Energy*, 2012, 37, 11602-11610.
194. Q. Xiang, J. Yu and M. Jaroniec, *The Journal of Physical Chemistry C*, 2011, 115, 7355-7363.
195. Z. Xing, Z. Chen, X. Zong and L. Wang, *Chemical Communications*, 2014, 50, 6762-6764.
196. Y. Chen, J. Li, Z. Hong, B. Shen, B. Lin and B. Gao, *Physical Chemistry Chemical Physics*, 2014, 16, 8106-8113.
197. Z. Chen, P. Sun, B. Fan, Z. Zhang and X. Fang, *The Journal of Physical Chemistry C*, 2014, 118, 7801-7807.
198. Z. Jiang, D. Liu, D. Jiang, W. Wei, K. Qian, M. Chen and J. Xie, *Dalton Transactions*, 2014, 43, 13792-13802.
199. H. Katsumata, Y. Tachi, T. Suzuki and S. Kaneco, *RSC Advances*, 2014, 4, 21405-21409.
200. J. Chen, S. Shen, P. Guo, P. Wu and L. Guo, *Journal of Materials Chemistry A*, 2014, 2, 4605-4612.
201. D. Jiang, L. Chen, J. Xie and M. Chen, *Dalton Transactions*, 2014, 43, 4878-4885.
202. L. Ge and C. Han, *Applied Catalysis B: Environmental*, 2012, 117–118, 268-274.
203. F. He, G. Chen, Y. Yu, S. Hao, Y. Zhou and Y. Zheng, *ACS Applied Materials & Interfaces*, 2014, 6, 7171-7179.
204. X. Zhang, L. Yu, C. Zhuang, T. Peng, R. Li and X. Li, *ACS Catalysis*, 2013, 4, 162-170.
205. H. Yan and Y. Huang, *Chemical Communications*, 2011, 47, 4168-4170.
206. S. Samanta, S. Martha and K. Parida, *ChemCatChem*, 2014, 6, 1453-1462.
207. J. Hong, Y. Wang, Y. Wang, W. Zhang and R. Xu, *ChemSusChem*, 2013, 6, 2263-2268.
208. Q. Li, B. Yue, H. Iwai, T. Kako and J. Ye, *The Journal of Physical Chemistry C*, 2010, 114, 4100-4105.
209. N. Bao, L. Shen, T. Takata, D. Lu and K. Domen, *Chem Lett*, 2006, 35.
210. H. Liu, J. Yang, J. Liang, Y. Huang and C. Tang, *Journal of the American Ceramic Society*, 2008, 91, 1287-1291.
211. Z. Jiang, F. Yang, N. Luo, B. T. Chu, D. Sun, H. Shi, T. Xiao and P. P. Edwards, *Chemical Communications*, 2008, 6372-6374.
212. J. Jitputti, S. Pavasupree, Y. Suzuki and S. Yoshikawa, *Japanese Journal of Applied Physics*, 2008, 47, 751.

213. Y. Li, T. Sasaki, Y. Shimizu and N. Koshizaki, *Journal of the American Chemical Society*, 2008, 130, 14755-14762.
214. W. W. Wang, Y. J. Zhu and L. X. Yang, *Advanced Functional Materials*, 2007, 17, 59-64.
215. E. C. Carroll, O. C. Compton, D. Madsen, F. E. Osterloh and D. S. Larsen, *The Journal of Physical Chemistry C*, 2008, 112, 2394-2403.
216. C. Ye, Y. Bando, G. Shen and D. Golberg, *The Journal of Physical Chemistry B*, 2006, 110, 15146-15151.
217. F. Andrew Frame, E. C. Carroll, D. S. Larsen, M. Sarahan, N. D. Browning and F. E. Osterloh, *Chemical Communications*, 2008, DOI: 10.1039/B718796C, 2206-2208.
218. D. Jing, R. Li, M. Liu and L. Guo, *International Journal of Nanotechnology*, 2011, 8, 446-457.
219. J. Lv, T. Kako, Z. Li, Z. Zou and J. Ye, *The Journal of Physical Chemistry C*, 2010, 114, 6157-6162.
220. H. Gyu Kim, J. Suk Jang, E. Duck Jeong, Y. Jae Suh and J. Sung Lee, *Chemical Communications*, 2009, 5889-5891.
221. A. C. Pradhan, S. Martha, S. Mahanta and K. Parida, *International Journal of Hydrogen Energy*, 2011, 36, 12753-12760.
222. P. Dhanasekaran, H. G. Salunke and N. M. Gupta, *The Journal of Physical Chemistry C*, 2012, 116, 12156-12164.
223. A. Tanaka, K. Hashimoto and H. Kominami, *Journal of the American Chemical Society*, 2013, 136, 586-589.
224. Y. Luo, X. Liu, X. Tang, Y. Luo, Q. Zeng, X. Deng, S. Ding and Y. Sun, *Journal of Materials Chemistry A*, 2014, 2, 14927-14939.
225. W. Xitao, L. Rong and W. Kang, *Journal of Materials Chemistry A*, 2014, 2, 8304-8313.
226. Q. Jia, A. Iwase and A. Kudo, *Chemical Science*, 2014, 5, 1513-1519.
227. S. Martha, K. H. Reddy and K. M. Parida, *Journal of Materials Chemistry A*, 2014, 2, 3621-3631.
228. Y. Jia, S. Shen, D. Wang, X. Wang, J. Shi, F. Zhang, H. Han and C. Li, *Journal of Materials Chemistry A*, 2013, 1, 7905-7912.
229. K. H. Reddy, S. Martha and K. M. Parida, *RSC Advances*, 2012, 2, 9423-9436.
230. K. M. Parida, A. Nashim and S. K. Mahanta, *Dalton Transactions*, 2011, 40, 12839-12845.
231. J. Liu, H. Zhang, D. Tang, X. Zhang, L. Yan, Y. Han, H. Huang, Y. Liu and Z. Kang, *ChemCatChem*, 2014, 6, 2634-2641.
232. T. Zhu, C. K. Nuo Peh, M. Hong and G. W. Ho, *Chemistry – A European Journal*, 2014, 20, 11505-11510.
233. G. Tian, Y. Chen, Z. Ren, C. Tian, K. Pan, W. Zhou, J. Wang and H. Fu, *Chemistry – An Asian Journal*, 2014, 9, 1291-1297.
234. A. Nashim , S. Martha and K. M. Parida *ChemCatChem*, 2013, 5, 2352-2359.
235. W. Cui, D. Guo, L. Liu, J. Hu, D. Rana and Y. Liang, *Catalysis Communications*, 2014, 48, 55-59.
236. L. Xu, L. Ni, W. Shi and J. Guan, *Chinese Journal of Catalysis*, 2012, 33, 1101-1108.

Highlights:

We reviewed recent advanced heterojunction semiconductors with various morphologies and chemical compositions, which are high potential for hydrogen production under visible light irradiation.

GRAPHICAL ABSTRACT: